Published in final edited form as:
J Neurosci Res. 2012 July ; 90(7): 1310–1323. doi:10.1002/jnr.23019.

Estrogen Treatment Prevents Gray Matter Atrophy in Experimental Autoimmune Encephalomyelitis

Allan J. MacKenzie-Graham[a,b,*], **Gilda A. Rinek**[a], **Andrea Avedisian**[a], **Laurie B. Morales**[b], **Elizabeth Umeda**[b], **Benoit Boulat**[c], **Russell E. Jacobs**[c], **Arthur W. Toga**[d], and **Rhonda R. Voskuhl**[b]

[a]Ahmanson-Lovelace Brain Mapping Center, Department of Neurology, University of California, Los Angeles, Los Angeles, California 90095-1769

[b]Multiple Sclerosis Program, Department of Neurology, University of California, Los Angeles, Los Angeles, California 90095-1769

[c]Beckman Institute, California Institute of Technology, 1200 E. California Blvd., Pasadena, California 91125-7400, USA

[d]Laboratory of Neuro Imaging, Department of Neurology, University of California, Los Angeles, Los Angeles, California 90095-1769

Abstract

Gray matter atrophy is an important correlate to clinical disability in multiple sclerosis (MS) and many treatment trials include atrophy as an outcome measure. Atrophy has been shown to occur in experimental autoimmune encephalomyelitis (EAE), the most commonly used animal model of MS. While the clinical severity of EAE is reduced in estrogen treated mice, it remains unknown whether estrogen treatment can reduce gray matter atrophy in EAE. In this study, mice with EAE were treated with either estrogen receptor (ER)-alpha ligand or ER-beta ligand, diffusion tensor images (DTI) were collected and neuropathology performed. DTI showed atrophy in the cerebellar gray matter of vehicle-treated EAE mice as compared to healthy controls, but not in ER-alpha or ER-beta ligand-treated EAE mice. Neuropathology demonstrated that Purkinje cell numbers were decreased in vehicle-treated EAE mice, while neither ER ligand-treated EAE groups showed a decrease. This is the first report of a neuroprotective therapy in EAE that unambiguously prevents gray matter atrophy while sparing a major neuronal cell type. Fractional anisotropy (FA) in the cerebellar white matter was decreased in vehicle-and ER-beta ligand-treated, but not in ER-alpha ligand-treated EAE mice. Inflammatory cell infiltration was increased in vehicle-and ER-beta ligand-treated, but not in ER-alpha ligand-treated EAE mice. Myelin staining was decreased in vehicle-treated EAE mice, and spared in both ER ligand-treated groups. This is consistent with decreased FA as a potential biomarker for inflammation rather than myelination or axonal damage in the cerebellum in EAE.

Keywords

dti; multiple sclerosis; mouse; ligand

[*]Correspondence to: Dr. Allan MacKenzie-Graham, Department of Neurology, David Geffen School of Medicine at UCLA, 710 Westwood Plaza, RNRC 4256, Los Angeles, CA 90095, Tel: (310) 447-4174; Fax: (310) 206-7282, amg@ucla.edu.

INTRODUCTION

Magnetic resonance imaging (MRI) measures of gray matter atrophy are an important characteristic of many neurodegenerative diseases, such as Alzheimer's disease, Parkinson's disease and multiple sclerosis (MS). In fact, there is a strong link between gray matter atrophy and disability in all of these diseases (Camicioli et al. 2003; Chard et al. 2002; Firbank et al. 2007). Whole brain atrophy was described in MS over a decade ago (Rudick et al. 1999) and several studies have since demonstrated a strong relationship between gray matter atrophy and disability (Amato et al. 2008; Calabrese et al. 2010; Ge et al. 2000). Indeed, gray matter atrophy is considered to be one of the most clinically relevant markers of MS disease progression (Bermel and Bakshi 2006; Fisher et al. 2002; van den Elskamp et al. 2010).

Diffusion tensor imaging (DTI) measures the diffusion of water molecules. When the mobility of a water molecule is not the same in all directions, its diffusion is said to be anisotropic. Anisotropic diffusion in the brain is due to underlying tissue anisotropy, with both myelin and axons contributing to the restriction of the free diffusion of water. Diffusion anisotropy is typically represented by an anisotropy index such as the fractional anisotropy (FA), the fraction of the "magnitude" of the diffusion along the principal axis of the diffusion tensor (Pierpaoli and Basser 1996). FA has been used as a marker for white matter tract integrity (Bammer et al. 2000; Filippi et al. 2001; Werring et al. 1999), reflecting the state of inflammation or myelination. Furthermore, it has been proposed that changes in the eigenvalues of the diffusion tensor may reflect either demyelination or axonal damage (Budde et al. 2009; Song et al. 2003).

Multiple sclerosis relapses decrease during late pregnancy and increase after birth, when female sex hormones are at high and low levels, respectively (Birk et al. 1990; Confavreux et al. 1998), suggesting a protective role (Voskuhl 2003). In EAE, both estriol and estradiol have been shown to be protective (Bebo et al. 2001; Jansson et al. 1994; Kim et al. 1999; Liu et al. 2003; Palaszynski et al. 2004; Papenfuss et al. 2011; Polanczyk et al. 2004). Numerous anti-inflammatory mechanisms appear to underlie the protective effect of estrogen in EAE (Ito et al. 2001; Subramanian et al. 2003; Zang et al. 2002). Further, work by our group has suggested a direct neuroprotective role for estrogens independent of these anti-inflammatory effects (Crawford et al. 2010; Spence et al. 2011; Tiwari-Woodruff et al. 2007).

The actions of estrogen are mediated primarily by nuclear estrogen receptors ER-alpha and ER-beta, although non-genomic membrane effects have also been described (Weiss and Gurpide 1988). Among the unresolved issues in the use of estrogens as neuroprotective agents are whether neuroprotective effects are primary, direct effects within the CNS, or secondary, indirect effects reducing inflammation into the CNS. While in most neurological disease models the protective effect of estrogen treatment has been shown to be mediated through ER-alpha and has been associated with anti-inflammatory effects (Merchenthaler et al. 2004; Morales et al. 2006; Suzuki et al. 2007; Suzuki et al. 2006), these are not mutually exclusive of direct neuroprotective mechanisms. In EAE, ER-alpha ligand treatment preserved myelin and neuronal staining while reducing inflammation in spinal cords, whereas ER-beta ligand treatment preserved myelin and neuronal staining without reducing inflammation (Tiwari-Woodruff et al. 2007). How these two similar, but distinct, neuroprotective treatments might influence the imaging outcomes of gray matter atrophy and diffusion anisotropy is unknown. Thus, the purpose of this study was to contrast the effects of EAE on gray matter atrophy and diffusion anisotropy in ER-alpha versus ER-beta ligand-treated EAE mice.

MATERIALS AND METHODS

Mice

Female C57BL/6 mice, 6 weeks old, were purchased from the Jackson Laboratory. All studies were performed in accordance with approval from the UCLA Office of Protection of Research Subjects.

Reagents

Estradiol (E2) was purchased from Sigma-Aldrich (St. Louis, MO). Propylpyrazole triol (ER-alpha ligand) and diarylpropionitrile (ER-beta ligand) were purchased from Tocris Bioscience (Ellisville, MO). Miglyol 812 N liquid oil was obtained from Sasol North America (Houston, TX). Myelin oligodendrocyte glycoprotein (MOG) peptide 35–55 was purchased at greater than 98% purity (Chiron Mimotopes, Emeryville, CA).

Animal Protocol

To remove the confound of endogenous circulating estrogens prior to estrogen treatment, female mice were ovariectomized following ketamine (100 mg/kg)/xylazine (10 mg/kg) anesthesia. The fur above the lateral dorsal back was removed and sterilized with betadine and alcohol scrubs. Bilateral incisions were made into the peritoneum. Sutures were placed on the fallopian tubes and the ovaries were removed. The peritoneal cavity and the abdominal musculature were sutured. The skin was secured with wound clips. Flunixin meglumine (2.5 mg/kg) was injected s.c. every 12 h for 2 days for pain. Enrofloxacin was added to the water for 5 days following surgery (45.4 mg/125 ml of water). Wound clips were removed 8–10 days following surgery.

The mice were allowed to recuperate for 10 days and then injected every other day with vehicle (10% ethanol and 90% miglyol) alone, E2, ER-alpha ligand or ER-beta ligand 7 days prior to EAE induction. E2, ER-alpha ligand and ER-beta ligand were dissolved in vehicle to give the final proper concentration of 0.04 mg/kg/d E2 (Jansson et al. 1994), 10 mg/kg/d ER-alpha ligand (Harris et al. 2002) and 8 mg/kg/d ER-beta ligand (Carswell et al. 2004). E2, ER-alpha ligand, ER-beta ligand or vehicle alone were given by daily subcutaneous injections along the midbackline and continued for the entire disease duration (up to 69 days after disease induction).

Experimental Autoimmune Encephalomyelitis

Mice were immunized with MOG peptide 35–55 (300 μg/mouse) and Mycobacterium tuberculosis (500 μg/mouse) emulsified in Complete Freund's Adjuvant subcutaneously, in a volume of 0.1 ml/mouse over two sites: the right draining inguinal and axillary lymph nodes. One week later a booster immunization was delivered subcutaneously, over the contralateral draining lymph nodes. Pertussis toxin (500 ng/mouse) (List Biological Laboratories, Inc., Campbell, CA) was injected intraperitoneally on days 0 and 2 (Liu et al. 2003; Suen et al. 1997). EAE was graded on a scale of 0 to 5, based on difficulty with ambulation, as described (Pettinelli and McFarlin 1981). A total of four independent EAE groups were used in this study.

Sample Preparation

Mice were anesthetized deeply using isofluorane. The mouse was then fixed by transcardiac perfusion using 30 ml of phosphate buffered saline (PBS) followed by 30 ml 4% paraformaldehyde (PFA) at 4°C. After death, the head was removed and rocked in 4% PFA overnight at 4°C. Soft tissue was removed and the skull (containing the brain) was rocked in 50 ml 0.01% sodium azide in PBS for 7.0 days at 4°C. The skull was then transferred to a 5

mM solution of gadoteridol (Prohance, Bracco Diagnostics Inc., Princeton NJ) and 0.01% sodium azide in PBS and rocked for 15 days at 4°C prior to MR imaging. Equilibration of the fixed brain in 5 mM gadoteridol solution significantly reduces the T1 of the sample and therefore reduces the total imaging time for a given resolution and target signal-to-noise ratio. All brains were equilibrated at room temperature for 8 hours immediately prior to imaging at 20°C.

Magnetic resonance imaging

All images were acquired using a vertical bore 11.7 T Bruker Avance DRX500 system (Bruker Biospin, Germany) equipped with a Micro2.5 imaging gradient set capable of a peak gradient strength of 1 T/m and a maximum slew rate of 12.5 kT/m/s. The skull (containing the brain) was secured in a Teflon holder and submerged in a perfluoropolyether (Fomblin, Solvay Solexis, Inc., Thorofare, NJ) within a 20 ml vial and imaged using a 35 mm birdcage transmit/receive volume resonator. All samples were equilibrated at room temperature prior to imaging. The ambient bore temperature was maintained at 20°C by thermostatically controlled airflow. Optimized second order shimming was achieved across the whole sample using the Bruker implementation of Fastmap (Gruetter 1993).

Diffusion-weighted images were acquired using a conventional pulsed-gradient spin echo (PGSE) sequence (TR/TE = 150 ms/11.6 ms, 256 × 150 × 130 matrix, 19.2 mm × 15 mm × 12 mm FOV, 80 Am isotropic voxel size, 1 average, diffusion gradient length: $\delta = 3$ ms, diffusion gradient separation: $\Delta = 5$ ms, diffusion gradient magnitude: $G_d = 750$ mT/m, nominal b-factor = 1450 s/mm^2). An optimized six point icosahedral encoding scheme (Hasan et al. 2001) was used for diffusion-weighted acquisitions with a single unweighted reference image for a total imaging time of 6 h.

Image Processing

Image processing was performed using a combination of freely distributed and in-house software implemented in Matlab (The Mathworks Inc., Natick MA). Reconstruction of the diffusion-weighted images included spatial radial Gaussian filtering (radial SD = 0.25 voxel) to smooth the coregistration cost-function and improve the SNR of all subsequent calculations. The six diffusion-weighted images were averaged to generate a high SNR isotropic diffusion-weighted image (iDWI) which could be used for both brain segmentation and image coregistration.

The apparent diffusion tensor was calculated conventionally by inversion of the encoding b-matrix (Mori 2007). Small shifts and rotations of the diffusion-weighted images were observed and ascribed to residual eddy currents from the high-amplitude diffusion encoding pulses persisting through the echo acquisition. Diffusion-weighted images were consequently registered to the diffusion unweighted image using a rigid-body transform under the assumption that the original diffusion encoding directions were exact and that the unweighted image best represents the true orientation of the mouse brain relative to the imaging gradient axes. The b-matrix for each diffusion encoding was determined by numerical simulation of the pulse sequence k-space trajectory in order to account for gradient cross-terms (Mattiello et al. 1997). Eigenvalues, eigenvectors, tensor trace and fractional anisotropy were calculated conventionally using built-in and custom Matlab functions.

iDWIs were skull-stripped using the Brain Surface Extractor (BSE) within BrainSuite 2 (Shattuck and Leahy 2001). Inaccuracies were corrected by manually editing the masks using BrainSuite 2. After skull-stripping, field inhomogeneities were corrected using N3 correction (Sled et al. 1998). A minimum deformation target (MDT) was produced as

described (Kochunov et al. 2001). Each of the images was then linearly aligned to the MDT with a 12-parameter full-affine transformation using Alignlinear (AIR 5.2.5) (Woods et al. 1998a; Woods et al. 1998b) and the least squares with intensity rescaling cost function followed by a 5th-order polynomial warp using Align_warp (AIR). The images were then resampled and averaged to produce the final minimum deformation atlas (MDA). The MDA was then aligned to a standard atlas (MacKenzie-Graham et al. 2004) to permit the direct comparison of images in a standard space. Automated image processing was performed in the LONI Pipeline Processing Environment (Rex et al. 2003) using a 8-processor Mac Pro computer (Apple Inc., Cupertino, CA).

Anatomical Delineations

A blinded expert neuroanatomist using BrainSuite 2 manually delineated anatomical structures on the MDA. Anatomical delineations included cerebellar cortex, cerebellar white matter, and olfactory bulb. Cerebellar cortex delineations rigorously excluded white matter and partial volume voxels. Anatomical delineations were based on the Mouse Atlas Project 2003 mouse brain atlas (MacKenzie-Graham et al. 2004) and assisted by the The Mouse Brain in Stereotaxic Coordinates 3rd edition (Franklin and Paxinos 2008).

Image Analysis

Images were spatially normalized with a 12-parameter full-affine transformation to register each image to the MDA using Alignlinear (AIR). In order to intensity normalize the images the alignment was performed with an intensity rescaling cost function. Align_warp (AIR) was used to compute 5th-order polynomial mappings of the MDA to each individual normalized brain. These mappings were then used to warp the anatomical delineations from the MDA to each of the individual images making up the atlas. Individual delineations were manually corrected and volumes recorded using BrainSuite 2.

Mean fractional anisotropy measurements were made by averaging the voxel values that were enclosed by the cerebellar white matter delineation using built-in and custom Matlab functions.

Tissue Preparation

After imaging, brains were removed from the skull and prepared for sectioning. 50 μm thick sagittal frozen sections were cut using a CM3050S cryostat (Leica Microsystems, Wetzlar, Germany). Free-floating sections were permeabilized in 0.3% Triton X-100 in PBS and blocked with 10% normal goat serum (Vector Laboratories, Burlingame, CA). White matter immunostaining was enhanced by treating sections with 95% ethanol/5% acetic acid for 15 minutes prior to permeabilization and blocking. Sections were incubated with primary antibodies in PBS solution containing 2% NGS for 2 hours at room temperature, then overnight at 4°C. The following primary antibodies were used: mouse anti-beta amyloid precursor protein (1:500; Abcam, Cambridge, MA), mouse anti-calbindin-2 (1:500; Sigma-Aldrich), rat anti-CD3 (1:1000; Millipore, Billerica, MA), rat anti-CD45 (1:1000; Millipore), rabbit anti-IBA-1 (1:1000; Wako, Richmond, VA), and rat anti-myelin basic protein (1:500; Millipore).

Fluorescence secondary antibody labeling included antibodies conjugated to Cy3 and Cy5 (Millipore). To assess the number of cells, 4',6'-diamidino-2-phenylindole dihydrochloride (DAPI; Invitrogen, Carlsbad, CA) was added for 15 minutes prior to final washes after secondary antibody addition. The sections were mounted on slides, dried, and coverslipped with fluoromount G (Fisher Scientific).

Chromogen immunohistochemistry was performed, after avidin-biotin block, by incubating with a biotinylated secondary antibody. A streptavidin-peroxidase conjugate was added, followed by the addition of 3,3'-diaminobenzidine (DAB; Vector Laboratories). The sections were mounted, dehydrated and coverslipped with Permount (Fisher Scientific, Pittsburgh, PA).

IgG-control experiments were performed for all primary antibodies, and no staining was observed under these conditions.

Microscopy and Analysis

Confocal images of immunostained sections were photographed using a spin-disc (Olympus, Center Valley, PA) and TCS-SP laser confocal microscope (Leica Microsystems) with a digital camera (Hamamatsu Photonics, Bridgewater, NJ). All images were collected using similar acquisition parameters. Photomicrographs of each representative experimental group were collected and analyzed with ImageJ software (v1.45a).

The degree of axonal damage, demyelination, and inflammation in cerebellar white and gray matter was assessed by quantifying anti-beta-APP, anti-MBP, and anti-CD45 staining by optical density. Confocal stacks of immunolabeled images from each animal were processed with a series of manual and automated procedures that included the following steps: (1) the images were oriented in the same direction, (2) the RGB channels of the images were split and converted to 8 bit gray images in Image J, (3) gray matter (granule cell, Purkinje cell and molecular layers) and white matter was manually delineated on the basis of DAPI staining, and (4) threshold gray matter and white matter density was calculated and reported as a percentage of total area.

Macrophages and microglia (IBA-1$^+$), T-lymphocytes (CD3$^+$) and Purkinje cells (calbindin-2$^+$), were quantified by counting cell bodies in 10X images of the entire cerebellum. Dehydration in chromogen-stained sections does not permit many z-planes to be available, so here we counted cells in a projected image. Three to five brain sections (50 μm thick) 200 μm apart were analyzed from each animal (ovarectomized vehicle-treated healthy controls: n = 5; ovarectomized vehicle-treated EAE mice: n = 5; ovarectomized ER-alpha ligand-treated EAE mice: n = 3; ovarectomized ER-beta ligand-treated EAE: n = 4). All sections counted were close to midline. Only cells with their entire nucleus present in the section were counted. Some of the animals imaged were excluded from the analysis due to incomplete perfusion or because the tissue was damaged.

Statistics

All results are presented as mean ± standard error of the mean (SEM) and statistical differences were determined by the Welch's t-test. ANOVAs and Welch's t-tests were performed in Excel (Microsoft, Redmond, WA). Comparisons were subject to *post hoc* multiple comparisons confounds, so the results of the Bonferroni correction ($p < \alpha/n$) were considered.

RESULTS

Post-mortem diffusion tensor imaging (DTI) scans were acquired from 30 female mice: 5 unmanipulated healthy controls, 5 ovarectomized vehicle-treated healthy controls, 5 ovarectomized vehicle-treated EAE mice, 5 ovarectomized ER-alpha ligand-treated EAE mice, 5 ovarectomized ER-beta ligand-treated EAE mice and 5 ovarectomized E2-treated EAE mice (as a positive control for estrogen treatment). The mice were sacrificed 69 days after disease induction (Fig. 1). There was a significant difference in the disease course between the ER-beta ligand-treated EAE mice and both the ER-alpha ligand- and E2-treated

EAE mice. Specifically, treatment with ER-alpha ligand and E2 completely blocked the entire disease course at both early and late time-points, while ER-beta ligand treatment only ameliorated disease late, but not early, consistent with previous reports (Gold et al. 2009; Tiwari-Woodruff et al. 2007; Tiwari-Woodruff and Voskuhl 2009).

A minimum deformation atlas (MDA) was constructed from the 30 isotropic diffusion-weighted images derived from the DT images collected (Fig. 2). The MDA then served as a target space for the spatial and intensity normalization of the original images, correcting both gross size and intensity differences. Following creation of this atlas, the olfactory bulbs, cerebellar cortices and cerebellar white matter were manually delineated on that atlas. The delineations were then warped onto the normalized images to produce standardized estimates of gray matter volumes in individual subjects.

Estrogen receptor ligand treatment of mice with EAE inhibits atrophy in the cerebellar cortex

We have previously demonstrated cerebellar atrophy in mice with EAE (MacKenzie-Graham et al. 2006; MacKenzie-Graham et al. 2009), an observation that has also been made in MS (Edwards et al. 1999; Iannucci et al. 1999; Liu et al. 1999). Our group has also demonstrated that estrogen-mediated disease protection in EAE may be due not only to the anti-inflammatory effects of estrogen, but also due to its neuroprotective properties which can be independent of reducing inflammation (Spence et al. 2011; Tiwari-Woodruff et al. 2007). Specifically, ER-alpha ligand treatment during EAE ameliorates clinical disease while reducing white matter inflammation in spinal cords, while ER-beta ligand treatment ameliorates clinical disease while not reducing inflammation. Therefore, using the methodology previously described to evaluate gray matter atrophy in mice with EAE (MacKenzie-Graham et al. 2009), we measured cerebellar cortical volumes in EAE mice that had been treated with vehicle, ER-alpha ligand or ER-beta ligand and compared them to healthy controls (Fig. 3). The volumes of the cerebellar cortices in the unmanipulated and ovarectomized healthy controls were not significantly different (data not shown). However, ovarectomized vehicle-treated EAE mice demonstrated an 8.4% decrease in the size of cerebellar cortex compared to ovarectomized vehicle-treated healthy controls ($p = 0.002$). ER-alpha ligand-treated ($p = 0.00009$), ER-beta ligand-treated ($p = 0.003$) or E2-treated ($p = 0.006$) EAE mice had cerebellar cortices that were significantly larger than vehicle-treated EAE mice and were not significantly different than those in vehicle-treated healthy controls. The volume of a control structure, the olfactory bulb, did not vary significantly in any of the groups. These data demonstrate that regardless of whether a given estrogen receptor ligand can reduce CNS inflammation, they each can prevent cerebellar cortical atrophy in EAE.

Estrogen receptor ligand treatment of mice with EAE inhibits Purkinje cell loss

In previous work we demonstrated cerebellar atrophy in mice with EAE over time (MacKenzie-Graham et al. 2006) and that a loss of Purkinje cells in EAE correlated strongly with that atrophy (MacKenzie-Graham et al. 2009). Furthermore, ER-alpha expression has been shown in the cerebellum (Shughrue et al. 1997; Simerly et al. 1990), specifically in Purkinje cells (Ikeda and Nagai 2006), and ER-beta has been shown to be expressed in the Purkinje cells (Jakab et al. 2001; Price and Handa 2000; Shughrue et al. 1997). Thus, we hypothesized that estrogen-mediated disease protection in mice with EAE might be due to not only the effects on inflammation and demyelination, but also due to the preservation of Purkinje cells in the cerebellum. This may in turn be associated with a prevention of cerebellar atrophy.

Calbindin-2 immunostaining demonstrated a disruption of the normal anatomy of the Purkinje and molecular layers of the cerebellar cortex in vehicle-treated EAE mice

compared to E2-treated EAE mice, ER-alpha ligand-treated EAE mice, ER-beta ligand-treated EAE mice and healthy controls (Fig. 4). Purkinje cell numbers were found to be 17.7% lower in vehicle-treated EAE mice than healthy controls ($p = 0.02$) (Fig. 5). Purkinje cell numbers were significantly greater in E2 and ER-alpha ligand-treated EAE mice as compared to vehicle-treated EAE mice ($p = 0.02$, $p = 0.002$), and were not significantly different from healthy controls. Purkinje cell numbers were also significantly preserved in ER-beta ligand-treated EAE mice as compared to vehicle-treated EAE mice ($p = 0.004$). Together these neuroimaging and neuropathological results suggest that gray matter atrophy as measured by MRI morphometry may be a biomarker for neuronal cell loss in EAE.

Fractional anisotropy is reduced in vehicle-treated and ER-beta ligand-treated, but not in estradiol-treated or ER-alpha ligand-treated mice with EAE

Fractional anisotropy has previously been used as a marker for white matter tract integrity (Bammer et al. 2000; Filippi et al. 2001; Werring et al. 1999). In order to evaluate white matter tract integrity, we measured the mean FA in the cerebellar white matter of mice with EAE that had been treated with vehicle only, E2, ER-alpha ligand or ER-beta ligand and compared them to healthy controls (Fig. 6). Vehicle-treated EAE mice demonstrated an 9.1% decrease in the FA of cerebellar white matter compared to controls ($p = 0.00001$). FA was significantly higher in ER-alpha ligand-treated ($p = 0.00006$) and E2-treated EAE mice ($p = 0.0004$) as compared to vehicle-treated EAE mice, and was not significantly different from healthy controls (Fig. 7). However, ER-beta ligand-treated EAE mice were not significantly different from vehicle-treated EAE mice, demonstrating an 8.0% decrease in FA as compared to controls ($p = 0.00004$). Together these neuroimaging and neuropathological results demonstrate that the treatment effects of atrophy versus FA may differ during EAE.

Estrogen receptor ligand treatment of mice with EAE preserves myelin in the cerebellum

Changes in fractional anisotropy may be due to changes in myelination. Thus, to further investigate differences observed in the FA of the cerebellar white matter in these mice, we measured myelin basic protein (MBP) expression. MBP immunoreactivity was measured to explore the state of myelin in both white and gray matter in the cerebellum. Healthy control tissue showed dense MBP staining in the central white matter tracts, with regular, parallel arrays of myelinated axons radiating into the granule cell layer (Fig. 8). White matter myelination was substantially greater than gray matter myelination. Quantification indicated that white and gray matter MBP immunoreactivity was significantly lower in vehicle-treated EAE mice than healthy controls ($p = 0.01$, $p = 0.0004$) (Fig. 9). White and gray matter MBP immunoreactivity was significantly greater in E2-treated EAE mice as compared to vehicle-treated EAE mice ($p = 0.0005$, $p = 0.008$), and not significantly different from healthy controls. Similarly, white and gray matter MBP immunoreactivity was significantly greater in ER-alpha ligand-treated EAE mice as compared to vehicle-treated EAE mice ($p = 0.006$, $p = 0.0006$), and not significantly different from healthy controls. Interestingly, white and gray matter MBP immunoreactivity was also significantly preserved in ER-beta ligand-treated EAE mice as compared to vehicle-treated EAE mice ($p = 0.01$, $p = 0.006$). The preservation of myelin staining in ER-beta ligand-treated mice who had a significant decrease in FA suggested that a neuropathology other than demyelination was underlying the decrease in FA.

Cerebellar inflammation in EAE is decreased with ER-alpha ligand, but not in ER-beta ligand treatment

Previous studies have shown that changes in FA can be caused not only by demyelination but also by inflammation. Thus, we next focussed our neuropathological analysis of the cerebella of mice with EAE on inflammation. Protein tyrosine phosphatase, receptor type C

(CD45) immunoreactivity is a commonly used measure of inflammation. Therefore, CD45 immunoreactivity was measured to explore the state of inflammation in both white and gray matter in the cerebellum. Healthy control tissue showed very little CD45 staining in either the white or gray matter (Fig. 10). Quantification indicated that white and gray matter CD45 immunoreactivity was significantly higher in vehicle-treated EAE mice as compared to healthy controls ($p = 0.00005$, $p = 0.001$) (Fig. 11A & B). White and gray matter CD45 immunoreactivity was significantly decreased in E2-treated as compared to vehicle-treated EAE mice ($p = 0.001$, $p = 0.00002$), and not significantly different from healthy controls. Similarly, white and gray matter CD45 immunoreactivity was significantly decreased in ER-alpha ligand-treated as compared to vehicle-treated EAE mice ($p = 0.001$, $p = 0.00002$), but not significantly different from healthy controls. In contrast, ER-beta ligand-treated EAE mice were not significantly different from vehicle-treated EAE mice, and demonstrated a significant increase in white and gray matter CD45 immunoreactivity as compared to healthy controls ($p = 0.0001$, $p = 0.0001$).

In order to better characterize the inflammatory response, we next stained with antibodies to ionized calcium binding adaptor molecule 1 (IBA1) and T-cell co-receptor (CD3). Anti-IBA1 stains cells of the macrophage/microglia lineage while anti-CD3 stains T-lymphocytes. $IBA1^+$ cell numbers were significantly higher in vehicle-treated EAE mice than healthy controls in both white and gray matter ($p = 0.000003$, $p = 0.00004$) (Fig. 11C & D). $IBA1^+$ cell numbers in white and gray matter were significantly lower in E2-treated EAE mice as compared to vehicle-treated EAE mice ($p = 0.000003$, $p = 0.00004$), and not significantly different from healthy controls. Similarly, $IBA1^+$ cell numbers in white and gray matter were significantly lower in ER-alpha ligand-treated EAE mice as compared to vehicle-treated EAE mice ($p = 0.000003$, $p = 0.00003$), and not significantly different from healthy controls. In contrast, ER-beta ligand-treated EAE mice were not significantly different from vehicle-treated EAE mice, and demonstrated significantly greater $IBA1^+$ cell numbers as compared to controls ($p = 0.000002$, $p = 0.00004$).

Quantification of $CD3^+$ staining indicated that T-lymphocyte numbers in white and gray matter were significantly higher in vehicle-treated EAE mice than healthy controls ($p = 0.000005$, $p = 0.00001$) (Fig. 11E & F). $CD3^+$ cell numbers in white and gray matter were significantly lower in E2-treated EAE mice as compared to vehicle-treated EAE mice ($p = 0.000005$, $p = 0.00003$), and not significantly different from controls. Similarly, $CD3^+$ cell numbers in white and gray matter were significantly lower in ER-alpha ligand-treated EAE mice as compared to vehicle-treated EAE mice ($p = 0.000005$, $p = 0.00003$), and not significantly different from controls. However, ER-beta ligand-treated EAE mice were not significantly different from vehicle-treated EAE mice, and demonstrated significantly higher $CD3^+$ cell numbers as compared to controls ($p = 0.000003$, $p = 0.00001$). There was no significant difference in $CD3^+$ cell number between vehicle-treated and ER-beta ligand-treated EAE mice.

Estrogen receptor ligand treatment of mice with EAE abrogates axonal damage in cerebellar white matter

Another possible cause for changes in fractional anisotropy may be due to axonal damage. Therefore we measured beta-amyloid precursor protein (beta-APP) expression, a sensitive marker of axonal injury (Ferguson et al. 1997). Healthy control tissue showed virtually no beta-APP staining in white matter tracts (Fig. 12). Quantification indicated that beta-APP immunoreactivity was much higher in vehicle-treated EAE mice than healthy controls ($p = 0.0001$) (Fig. 13). Beta-APP immunoreactivity was significantly lower in E2- and ER-alpha ligand-treated EAE mice as compared to vehicle-treated EAE mice ($p = 0.0001$, $p = 0.0001$). Interestingly, beta-APP immunoreactivity was also significantly lower in ER-beta ligand-treated EAE mice as compared to vehicle-treated EAE mice ($p = 0.0002$).

Together these neuroimaging and neuropathological results demonstrate that the ability of a given treatment to reduce inflammation in a given substructure coincides with its ability to preserve FA within the same substructure in EAE. These results are summarized in Table 1.

DISCUSSION

Most therapies for MS have been developed to reduce inflammation. Interferon-beta, glatiramer acetate and mitoxantrone have considerably improved the therapeutic options for patients with MS. These anti-inflammatory agents reduce relapse rates and reduce the appearance of contrast-enhancing lesions. However, their efficacy in preventing accumulation of disability, slowing gray matter atrophy and their impact on disease progression has been somewhat disappointing (Trojano et al. 2006; Van der Walt et al. 2010).

In this study, we have contrasted effects of treatment with ER-alpha versus ER-beta ligands on gray matter atrophy in EAE, the MS model with a known pathogenic role for both inflammation and neurodegeneration. Morphometry demonstrated that atrophy was abrogated in ER-alpha ligand-, ER-beta ligand- and E2-treated EAE mice. Similarly, Purkinje cell numbers were preserved in ER-alpha ligand-, ER-beta ligand and E2-treated EAE mice. Interestingly, the mean fractional anisotropy was preserved in ER-alpha ligand- and E2-treated EAE mice, but not in ER-beta ligand-treated EAE mice. Immunohistochemistry demonstrated that white and gray matter myelin staining was preserved in both ER-alpha ligand-, ER-beta ligand- and E2-treated EAE mice, however, cerebellar inflammation in EAE was decreased in ER-alpha ligand- and E2-treated, but not in ER-beta ligand-treated EAE mice. Together, we have demonstrated that DTI can visualize treatment effects on different elements of the pathology of EAE. Specifically, atrophy is a biomarker for Purkinje cell number and FA can be used as a biomarker for inflammation in the cerebellum in EAE. Both proved to be be highly informative in assessing the effects of treatments on disease.

Since the variability was low in both clinical scores and mean cerebellar cortex volumes within each treatment group, one could not assess whether mice with worse clinical scores had more atrophy within a given treatment group. However, between group comparisons revealed that vehicle-treated mice with EAE indeed had both worse clinical scores and more atrophy than E2-, ER-alpha ligand-, or ER-beta ligand-treated mice with EAE. FA values were also characterized by low variability within groups. In contrast to cerebellar volumes, between group comparisons of cerebellar FA did not show an association with disease. This was principally due to the fact that the ER beta ligand treated group demonstrated disease amelioration paired with a low FA.

Our results show for the first time that estrogen treatment can prevent gray matter atrophy and preserve Purkinje cells in the cerebellum during EAE. The prevention of the loss of this major neuronal cell type in EAE is significant due to their functional relevance. Purkinje cells are intimately involved in motor activity and represent the only output pathway of the cerebellar cortex (Parent 1996). The ER-beta ligand treatment effect was clearly not mediated by a reduction of cerebellar inflammation, since there was no significant difference in CD45 expression, $IBA1^+$ cell number nor $CD3^+$ cell number between ER-beta ligand-treated and vehicle-treated EAE mice. What remains unknown is whether the neuroprotective effect of ER-beta ligand treatment is mediated through binding to ER-beta receptors on neurons, oligodendrocytes, or astrocytes, because all of these CNS cell types have been shown to express ER-beta in vivo (Platania et al. 2003). In fact, it is likely that there is a direct effect of estrogen receptor beta ligand treatment on Purkinje cell survival

since Purkinje cells have been shown to express estrogen receptor beta (Jakab et al. 2001; Price and Handa 2000; Sakamoto et al. 2003; Shughrue et al. 1997).

Though our results are strongly suggestive of a direct effect of estrogen on Purkinje cells, we cannot eliminate the possibility that the estrogen effect is mediated by other cells such as astrocytes (Spence et al. 2011) or even non-CNS cells. Propyl pyrazole triol (ER-alpha ligand) and diarylpropionitrile (ER-beta ligand) are estrogen receptor agonists with well characterized affinities for ER-alpha and ER-beta respectively (Harrington et al. 2003; Meyers et al. 2001), and previous studies with knockout mice(Morales et al. 2006) have established the selectivity and responsiveness of these ligands in vivo. Results obtained from this approach should complement studies with knockout mice and help to further expand our appreciation of the complexities of estrogen action.

A decrease in FA has previously been reported in dysmyelinating shiverer mice compared to normal controls thereby suggesting that FA is indicative of the level of myelination (Tyszka et al. 2006). Our finding that the fractional anisotropy is decreased in mice with EAE was similarly reported using a related measure, relative anisotropy in EAE (Budde et al. 2009). Consistent with our results, whereby decreases in FA were independent of myelin staining, Budde et al. found no correlation between relative anisotropy and MBP staining in EAE (Budde et al. 2009). Differences between these two reports involve the relationship between FA and inflammation. Budde et al. demonstrated a weak correlation between relative anisotropy and cellular infiltrate. In contrast, our findings suggested that decreases in FA are related to inflammation, since both vehicle- and ER-beta ligand-treated EAE mice demonstrated a decrease in FA and both vehicle- and ER-beta ligand-treated EAE mice demonstrated increased inflammatory cell infiltration. One possible explanation for the discrepancy in our findings could be differences in staining. We stained for very specific markers of inflammation (CD45, CD3 and IBA1), whereas Budde et al. used a non-specific nuclear stain ($DAPI^{+}$) to measure inflammation indirectly. Second, and perhaps more importantly, we evaluated FA in the cerebellar white matter, while Budde et al. evaluated white matter tracts of the spinal cord. The diffusion anisotropy in the cerebellar white matter is lower than in the white matter tracts of the spinal cord in normals. The cerebellar white matter contains many white matter tracts traveling in different directions; it is comprised of the cerebellodentatorubral, cerebellodentatothallamic, cerebellovestibular, cuneocerebellar, olivocerebellar, pontocerebellar, reticulcerebellar, spinocerebellar, trigeminocerebellar and vestibulospinal fiber tracts, not to mention the myelinated Purkinje cell axons that project to the deep cerebellar nuclei. It is possible that the FA in the white matter in the cerebellum is more sensitive to inflammation than in the highly organized spinal cord. Lastly, we calculated the mean FA for the entire cerebellar white matter and counted infiltrating cells across the entire cerebellum, whereas Budde et al. focussed on specific areas of the spinal cord and evaluated their correlations on a pixel-by-pixel basis. Together these findings suggest that FA may be a sensitive biomarker for inflammation depending on the CNS area of study.

In an effort to better understand the pathology in MS lesions, DTI has proven to be a valuable tool. Anisotropy measures have commonly been used as biomarkers for demyelination and axonal damage. For example, decreased FA has been shown to be more pronounced in lesions than in the normal appearing white matter (NAWM); though its values are highly heterogeneous. This has been interpreted as indicating the variable degrees of tissue damage occurring within MS lesions (Filippi et al. 2001). However, FA is always lower in contrast-enhancing lesions, especially ring-enhancing lesions (Bammer et al. 2000), as compared to non-enhancing lesions, the latter of which are thought to reflect demyelination and axonal damage with minimal inflammatory infiltrate (Castriota-Scanderbeg et al. 2003; Filippi et al. 2001). Contrast enhancement is thought to be due to

blood–brain barrier breakdown secondary to inflammatory cell infiltration. Histological studies lend support to this idea, demonstrating that lesions with enhancement show inflammatory activity, either macrophage infiltration (Nesbit et al. 1991) or perivascular lymphocytic infiltration (Katz et al. 1993). Our findings demonstrate that inflammation can play an important role in the decrease of FA in the white matter of mice with EAE and suggests that the use of decreased FA as a biomarker for demyelination and axonal damage (Hesseltine et al. 2006) should be tempered with the understanding that inflammation may be playing a major role in the observed decrease.

In summary, we have found that treatment of mice with EAE with either estrogen receptor alpha or estrogen receptor beta ligand prevents gray matter atrophy and preserves a major neuronal population. This finding has implications for treatment in MS, suggesting that early treatment with neuroprotective agents may help spare patients from permanent clinical disability and irreversible neuronal damage. Further, multimodal approaches using neuroimaging combined with immunohistochemistry in disease models suggests that DTI can indeed differentiate between different treatment mechanisms.

Acknowledgments

Contract grant sponsor: The National Multiple Sclerosis Society FG 1759A1/1 (AMG), RG 4033, RG 4364, and CA 1028 (RRV); Contract grant sponsor: The National Institutes of Health P41 RR013642 (AWT) and K24 NS062117 (RRV); Contract grant sponsor: The National Institute of Biomedical Imaging and Bioengineering R01 EB000993 (REJ); Contract grant sponsor: The Skirball Foundation (RRV); Contract grant sponsor: The Hilton Foundation (RRV); Contract grant sponsor: The Sherak Family Foundation (RRV).

BIBLIOGRAPHY

Amato MP, Portaccio E, Stromillo ML, Goretti B, Zipoli V, Siracusa G, Battaglini M, Giorgio A, Bartolozzi ML, Guidi L, Sorbi S, Federico A, De Stefano N. Cognitive assessment and quantitative magnetic resonance metrics can help to identify benign multiple sclerosis. Neurology. 2008; 71(9): 632–638. [PubMed: 18725589]

Bammer R, Augustin M, Strasser-Fuchs S, Seifert T, Kapeller P, Stollberger R, Ebner F, Hartung HP, Fazekas F. Magnetic resonance diffusion tensor imaging for characterizing diffuse and focal white matter abnormalities in multiple sclerosis. Magn Reson Med. 2000; 44(4):583–591. [PubMed: 11025514]

Bebo BF Jr, Fyfe-Johnson A, Adlard K, Beam AG, Vandenbark AA, Offner H. Low-dose estrogen therapy ameliorates experimental autoimmune encephalomyelitis in two different inbred mouse strains. Journal of Immunology. 2001; 166:2080–2089.

Bermel RA, Bakshi R. The measurement and clinical relevance of brain atrophy in multiple sclerosis. Lancet Neurol. 2006; 5(2):158–170. [PubMed: 16426992]

Birk K, Ford C, Smeltzer S, Ryan D, Miller R, Rudick RA. The clinical course of multiple sclerosis during pregnancy and the puerperium. Arch Neurol. 1990; 47(7):738–742. [PubMed: 1972617]

Budde MD, Xie M, Cross AH, Song SK. Axial diffusivity is the primary correlate of axonal injury in the experimental autoimmune encephalomyelitis spinal cord: a quantitative pixelwise analysis. J Neurosci. 2009; 29(9):2805–2813. [PubMed: 19261876]

Calabrese M, Mattisi I, Rinaldi F, Favaretto A, Atzori M, Bernardi V, Barachino L, Romualdi C, Rinaldi L, Perini P, Gallo P. Magnetic resonance evidence of cerebellar cortical pathology in multiple sclerosis. J Neurol Neurosurg Psychiatry. 2010; 81(4):401–404. [PubMed: 19965849]

Camicioli R, Moore MM, Kinney A, Corbridge E, Glassberg K, Kaye JA. Parkinson's disease is associated with hippocampal atrophy. Mov Disord. 2003; 18(7):784–790. [PubMed: 12815657]

Carswell HV, Macrae IM, Gallagher L, Harrop E, Horsburgh KJ. Neuroprotection by a selective estrogen receptor beta agonist in a mouse model of global ischemia. Am J Physiol Heart Circ Physiol. 2004; 287(4):H1501–H1504. [PubMed: 15155257]

Castriota-Scanderbeg A, Fasano F, Hagberg G, Nocentini U, Filippi M, Caltagirone C. Coefficient D(av) is more sensitive than fractional anisotropy in monitoring progression of irreversible tissue

damage in focal nonactive multiple sclerosis lesions. AJNR Am J Neuroradiol. 2003; 24(4):663–670. [PubMed: 12695200]

Chard DT, Griffin CM, Parker GJ, Kapoor R, Thompson AJ, Miller DH. Brain atrophy in clinically early relapsing-remitting multiple sclerosis. Brain. 2002; 125(Pt 2):327–337. [PubMed: 11844733]

Confavreux C, Hutchinson M, Hours MM, Cortinovis-Tourniaire P, Moreau T. Rate of pregnancy-related relapse in multiple sclerosis. Pregnancy in Multiple Sclerosis Group [see comments]. New England Journal of Medicine. 1998; 339(5):285–291. [PubMed: 9682040]

Crawford DK, Mangiardi M, Song B, Patel R, Du S, Sofroniew MV, Voskuhl RR, Tiwari-Woodruff SK. Oestrogen receptor beta ligand: a novel treatment to enhance endogenous functional remyelination. Brain. 2010; 133(10):2999–3016. [PubMed: 20858739]

Edwards SG, Gong QY, Liu C, Zvartau ME, Jaspan T, Roberts N, Blumhardt LD. Infratentorial atrophy on magnetic resonance imaging and disability in multiple sclerosis. Brain. 1999; 122(Pt 2):291–301. [PubMed: 10071057]

Ferguson B, Matyszak MK, Esiri MM, Perry VH. Axonal damage in acute multiple sclerosis lesions. Brain. 1997; 120(Pt 3):393–399. [PubMed: 9126051]

Filippi M, Cercignani M, Inglese M, Horsfield MA, Comi G. Diffusion tensor magnetic resonance imaging in multiple sclerosis. Neurology. 2001; 56(3):304–311. [PubMed: 11171893]

Firbank MJ, Blamire AM, Krishnan MS, Teodorczuk A, English P, Gholkar A, Harrison R, O'Brien JT. Atrophy is associated with posterior cingulate white matter disruption in dementia with Lewy bodies and Alzheimer's disease. Neuroimage. 2007

Fisher E, Rudick RA, Simon JH, Cutter G, Baier M, Lee JC, Miller D, Weinstock-Guttman B, Mass MK, Dougherty DS, Simonian NA. Eight-year follow-up study of brain atrophy in patients with MS. Neurology. 2002; 59(9):1412–1420. [PubMed: 12427893]

Franklin, KBJ.; Paxinos, G. The Mouse Brain in Stereotaxic Coordinates. New York: Academic Press; 2008.

Ge Y, Grossman RI, Udupa JK, Wei L, Mannon LJ, Polansky M, Kolson DL. Brain atrophy in relapsing-remitting multiple sclerosis and secondary progressive multiple sclerosis: longitudinal quantitative analysis. Radiology. 2000; 214(3):665–670. [PubMed: 10715027]

Gold SM, Sasidhar MV, Morales LB, Du S, Sicotte NL, Tiwari-Woodruff SK, Voskuhl RR. Estrogen treatment decreases matrix metalloproteinase (MMP)-9 in autoimmune demyelinating disease through estrogen receptor alpha (ERalpha). Lab Invest. 2009; 89(10):1076–1083. [PubMed: 19668239]

Gruetter R. Automatic, localized in vivo adjustment of all first- and second-order shim coils. Magn Reson Med. 1993; 29(6):804–811. [PubMed: 8350724]

Harrington WR, Sheng S, Barnett DH, Petz LN, Katzenellenbogen JA, Katzenellenbogen BS. Activities of estrogen receptor alpha- and beta-selective ligands at diverse estrogen responsive gene sites mediating transactivation or transrepression. Mol Cell Endocrinol. 2003; 206(1–2):13–22. [PubMed: 12943986]

Harris HA, Katzenellenbogen JA, Katzenellenbogen BS. Characterization of the biological roles of the estrogen receptors, ERalpha and ERbeta, in estrogen target tissues in vivo through the use of an ERalpha-selective ligand. Endocrinology. 2002; 143(11):4172–4177. [PubMed: 12399409]

Hasan KM, Parker DL, Alexander AL. Comparison of gradient encoding schemes for diffusion-tensor MRI. J Magn Reson Imaging. 2001; 13(5):769–780. [PubMed: 11329200]

Hesseltine SM, Law M, Babb J, Rad M, Lopez S, Ge Y, Johnson G, Grossman RI. Diffusion tensor imaging in multiple sclerosis: assessment of regional differences in the axial plane within normal-appearing cervical spinal cord. AJNR Am J Neuroradiol. 2006; 27(6):1189–1193. [PubMed: 16775261]

Iannucci G, Minicucci L, Rodegher M, Sormani MP, Comi G, Filippi M. Correlations between clinical and MRI involvement in multiple sclerosis: assessment using T(1), T(2) and MT histograms. J Neurol Sci. 1999; 171(2):121–129. [PubMed: 10581378]

Ikeda Y, Nagai A. Differential expression of the estrogen receptors alpha and beta during postnatal development of the rat cerebellum. Brain Res. 2006; 1083(1):39–49. [PubMed: 16542644]

Ito A, Bebo BF Jr, Matejuk A, Zamora A, Silverman M, Fyfe-Johnson A, Offner H. Estrogen treatment down-regulates TNF-alpha production and reduces the severity of experimental

autoimmune encephalomyelitis in cytokine knockout mice. J Immunol. 2001; 167(1):542–552. [PubMed: 11418693]

Jakab RL, Wong JK, Belcher SM. Estrogen receptor beta immunoreactivity in differentiating cells of the developing rat cerebellum. J Comp Neurol. 2001; 430(3):396–409. [PubMed: 11169476]

Jansson L, Olsson T, Holmdahl R. Estrogen induces a potent suppression of experimental autoimmune encephalomyelitis and collagen-induced arthritis in mice. Journal of Neuroimmunology. 1994; 53(2):203–207. [PubMed: 8071434]

Katz D, Taubenberger JK, Cannella B, McFarlin DE, Raine CS, McFarland HF. Correlation between magnetic resonance imaging findings and lesion development in chronic, active multiple sclerosis. Ann Neurol. 1993; 34(5):661–669. [PubMed: 8239560]

Kim S, Liva SM, Dalal MA, Verity MA, Voskuhl RR. Estriol ameliorates autoimmune demyelinating disease: implications for multiple sclerosis. Neurology. 1999; 52(6):1230–1238. [PubMed: 10214749]

Kochunov P, Lancaster JL, Thompson P, Woods R, Mazziotta J, Hardies J, Fox P. Regional spatial normalization: toward an optimal target. J Comput Assist Tomogr. 2001; 25(5):805–816. [PubMed: 11584245]

Liu C, Edwards S, Gong Q, Roberts N, Blumhardt LD. Three dimensional MRI estimates of brain and spinal cord atrophy in multiple sclerosis. J Neurol Neurosurg Psychiatry. 1999; 66(3):323–330. [PubMed: 10084530]

Liu HB, Loo KK, Palaszynski K, Ashouri J, Lubahn DB, Voskuhl RR. Estrogen receptor alpha mediates estrogen's immune protection in autoimmune disease. J Immunol. 2003; 171(12):6936–6940. [PubMed: 14662901]

MacKenzie-Graham A, Lee EF, Dinov ID, Bota M, Shattuck DW, Ruffins S, Yuan H, Konstantinidis F, Pitiot A, Ding Y, Hu G, Jacobs RE, Toga AW. A multimodal, multidimensional atlas of the C57BL/6J mouse brain. J Anat. 2004; 204(2):93–102. [PubMed: 15032916]

MacKenzie-Graham A, Tinsley MR, Shah KP, Aguilar C, Strickland LV, Boline J, Martin M, Morales L, Shattuck DW, Jacobs RE, Voskuhl RR, Toga AW. Cerebellar cortical atrophy in experimental autoimmune encephalomyelitis. Neuroimage. 2006; 32(3):1016–1023. [PubMed: 16806982]

MacKenzie-Graham A, Tiwari-Woodruff SK, Sharma G, Aguilar C, Vo KT, Strickland LV, Morales L, Fubara B, Martin M, Jacobs RE, Johnson GA, Toga AW, Voskuhl RR. Purkinje cell loss in experimental autoimmune encephalomyelitis. Neuroimage. 2009; 48(4):637–651. [PubMed: 19589388]

Mattiello J, Basser PJ, Le Bihan D. The b matrix in diffusion tensor echo-planar imaging. Magn Reson Med. 1997; 37(2):292–300. [PubMed: 9001155]

Merchenthaler I, Lane MV, Numan S, Dellovade TL. Distribution of estrogen receptor alpha and beta in the mouse central nervous system: in vivo autoradiographic and immunocytochemical analyses. J Comp Neurol. 2004; 473(2):270–291. [PubMed: 15101093]

Meyers MJ, Sun J, Carlson KE, Marriner GA, Katzenellenbogen BS, Katzenellenbogen JA. Estrogen receptor-beta potency-selective ligands: structure-activity relationship studies of diarylpropionitriles and their acetylene and polar analogues. J Med Chem. 2001; 44(24):4230–4251. [PubMed: 11708925]

Morales LB, Loo KK, Liu HB, Peterson C, Tiwari-Woodruff S, Voskuhl RR. Treatment with an estrogen receptor alpha ligand is neuroprotective in experimental autoimmune encephalomyelitis. J Neurosci. 2006; 26(25):6823–6833. [PubMed: 16793889]

Mori, S. Introduction to diffusion tensor imaging. Vol. xiii. Amsterdam; Boston: Elsevier; 2007. p. 176

Nesbit GM, Forbes GS, Scheithauer BW, Okazaki H, Rodriguez M. Multiple sclerosis: histopathologic and MR and/or CT correlation in 37 cases at biopsy and three cases at autopsy. Radiology. 1991; 180(2):467–474. [PubMed: 2068314]

Palaszynski KM, Liu H, Loo KK, Voskuhl RR. Estriol treatment ameliorates disease in males with experimental autoimmune encephalomyelitis: implications for multiple sclerosis. J Neuroimmunol. 2004; 149(1–2):84–89. [PubMed: 15020068]

Papenfuss TL, Powell ND, McClain MA, Bedarf A, Singh A, Gienapp IE, Shawler T, Whitacre CC. Estriol Generates Tolerogenic Dendritic Cells In Vivo That Protect against Autoimmunity. J Immunol. 2011; 186(6):3346–3355. [PubMed: 21317386]

Parent, A. Carpenter's Human Neuroanatomy. Media, PA: Williams & Wilkins; 1996.

Pettinelli CB, McFarlin DE. Adoptive transfer of experimental allergic encephalomyelitis in SJL/J mice after in vitro activation of lymph node cells by myelin basic protein: requirement for Lyt 1+ 2- T lymphocytes. J Immunol. 1981; 127(4):1420–1423. [PubMed: 6168690]

Pierpaoli C, Basser PJ. Toward a quantitative assessment of diffusion anisotropy. Magn Reson Med. 1996; 36(6):893–906. [PubMed: 8946355]

Platania P, Laureanti F, Bellomo M, Giuffrida R, Giuffrida-Stella AM, Catania MV, Sortino MA. Differential expression of estrogen receptors alpha and beta in the spinal cord during postnatal development: localization in glial cells. Neuroendocrinology. 2003; 77(5):334–340. [PubMed: 12806179]

Polanczyk MJ, Carson BD, Subramanian S, Afentoulis M, Vandenbark AA, Ziegler SF, Offner H. Cutting edge: estrogen drives expansion of the CD4+CD25+ regulatory T cell compartment. J Immunol. 2004; 173(4):2227–2230. [PubMed: 15294932]

Price RH Jr, Handa RJ. Expression of estrogen receptor-beta protein and mRNA in the cerebellum of the rat. Neurosci Lett. 2000; 288(2):115–118. [PubMed: 10876074]

Rex DE, Ma JQ, Toga AW. The LONI Pipeline Processing Environment. Neuroimage. 2003; 19(3): 1033–1048. [PubMed: 12880830]

Rudick RA, Fisher E, Lee JC, Simon J, Jacobs L. Use of the brain parenchymal fraction to measure whole brain atrophy in relapsing-remitting MS. Multiple Sclerosis Collaborative Research Group. Neurology. 1999; 53(8):1698–1704. [PubMed: 10563615]

Sakamoto H, Mezaki Y, Shikimi H, Ukena K, Tsutsui K. Dendritic growth and spine formation in response to estrogen in the developing Purkinje cell. Endocrinology. 2003; 144(10):4466–4477. [PubMed: 12960093]

Shattuck DW, Leahy RM. Automated graph-based analysis and correction of cortical volume topology. IEEE Trans Med Imaging. 2001; 20(11):1167–1177. [PubMed: 11700742]

Shughrue PJ, Lane MV, Merchenthaler I. Comparative distribution of estrogen receptor-alpha and -beta mRNA in the rat central nervous system. J Comp Neurol. 1997; 388(4):507–525. [PubMed: 9388012]

Simerly RB, Chang C, Muramatsu M, Swanson LW. Distribution of androgen and estrogen receptor mRNA-containing cells in the rat brain: an in situ hybridization study. J Comp Neurol. 1990; 294(1):76–95. [PubMed: 2324335]

Skare S, Li T, Nordell B, Ingvar M. Noise considerations in the determination of diffusion tensor anisotropy. Magn Reson Imaging. 2000; 18(6):659–669. [PubMed: 10930775]

Sled JG, Zijdenbos AP, Evans AC. A nonparametric method for automatic correction of intensity nonuniformity in MRI data. IEEE Trans Med Imaging. 1998; 17(1):87–97. [PubMed: 9617910]

Song SK, Sun SW, Ju WK, Lin SJ, Cross AH, Neufeld AH. Diffusion tensor imaging detects and differentiates axon and myelin degeneration in mouse optic nerve after retinal ischemia. Neuroimage. 2003; 20(3):1714–1722. [PubMed: 14642481]

Spence RD, Hamby ME, Umeda E, Itoh N, Du S, Wisdom AJ, Cao Y, Bondar G, Lam J, Ao Y, Sandoval F, Suriany S, Sofroniew MV, Voskuhl RR. Neuroprotection mediated through estrogen receptor-alpha in astrocytes. Proc Natl Acad Sci U S A. 2011; 108(21):8867–8872. [PubMed: 21555578]

Subramanian S, Matejuk A, Zamora A, Vandenbark AA, Offner H. Oral feeding with ethinyl estradiol suppresses and treats experimental autoimmune encephalomyelitis in SJL mice and inhibits the recruitment of inflammatory cells into the central nervous system. J Immunol. 2003; 170(3):1548–1555. [PubMed: 12538720]

Suen WE, Bergman CM, Hjelmstrom P, Ruddle NH. A critical role for lymphotoxin in experimental allergic encephalomyelitis. J Exp Med. 1997; 186(8):1233–1240. [PubMed: 9334362]

Suzuki S, Brown CM, Dela Cruz CD, Yang E, Bridwell DA, Wise PM. Timing of estrogen therapy after ovariectomy dictates the efficacy of its neuroprotective and antiinflammatory actions. Proc Natl Acad Sci U S A. 2007; 104(14):6013–6018. [PubMed: 17389368]

Suzuki S, Brown CM, Wise PM. Mechanisms of neuroprotection by estrogen. Endocrine. 2006; 29(2): 209–215. [PubMed: 16785597]

Tiwari-Woodruff S, Morales LB, Lee R, Voskuhl RR. Differential neuroprotective and antiinflammatory effects of estrogen receptor (ER){alpha} and ER{beta} ligand treatment. Proc Natl Acad Sci U S A. 2007

Tiwari-Woodruff S, Voskuhl RR. Neuroprotective and anti-inflammatory effects of estrogen receptor ligand treatment in mice. J Neurol Sci. 2009; 286(1–2):81–85. [PubMed: 19442988]

Trojano M, Russo P, Fuiani A, Paolicelli D, Di Monte E, Granieri E, Rosati G, Savettieri G, Comi G, Livrea P, Group MS. The Italian Multiple Sclerosis Database Network (MSDN): the risk of worsening according to IFNbeta exposure in multiple sclerosis. Mult Scler. 2006; 12(5):578–585. [PubMed: 17086903]

Tyszka JM, Readhead C, Bearer EL, Pautler RG, Jacobs RE. Statistical diffusion tensor histology reveals regional dysmyelination effects in the shiverer mouse mutant. Neuroimage. 2006; 29(4): 1058–1065. [PubMed: 16213163]

van den Elskamp IJ, Boden B, Dattola V, Knol DL, Filippi M, Kappos L, Fazekas F, Wagner K, Pohl C, Sandbrink R, Polman CH, Uitdehaag BM, Barkhof F. Cerebral atrophy as outcome measure in short-term phase 2 clinical trials in multiple sclerosis. Neuroradiology. 2010; 52(10):875–881. [PubMed: 20049424]

Van der Walt A, Butzkueven H, Kolbe S, Marriott M, Alexandrou E, Gresle M, Egan G, Kilpatrick T. Neuroprotection in multiple sclerosis: a therapeutic challenge for the next decade. Pharmacol Ther. 2010; 126(1):82–93. [PubMed: 20122960]

Voskuhl RR. Hormone-based therapies in MS. Int MS J. 2003; 10(2):60–66. [PubMed: 14561384]

Weiss DJ, Gurpide E. Non-genomic effects of estrogens and antiestrogens. J Steroid Biochem. 1988; 31(4B):671–676. [PubMed: 2848981]

Werring DJ, Clark CA, Barker GJ, Thompson AJ, Miller DH. Diffusion tensor imaging of lesions and normal-appearing white matter in multiple sclerosis. Neurology. 1999; 52(8):1626–1632. [PubMed: 10331689]

Woods RP, Grafton ST, Holmes CJ, Cherry SR, Mazziotta JC. Automated image registration: I. General methods and intrasubject, intramodality validation. J Comput Assist Tomogr. 1998a; V22(N1):139–152.

Woods RP, Grafton ST, Watson JD, Sicotte NL, Mazziotta JC. Automated image registration: II. Intersubject validation of linear and nonlinear models. J Comput Assist Tomogr. 1998b; 22(1): 153–165. [PubMed: 9448780]

Zang YC, Halder JB, Hong J, Rivera VM, Zhang JZ. Regulatory effects of estriol on T cell migration and cytokine profile: inhibition of transcription factor NF-kappa B. Neuroimmunol. 2002; 124(1–2):106–114.

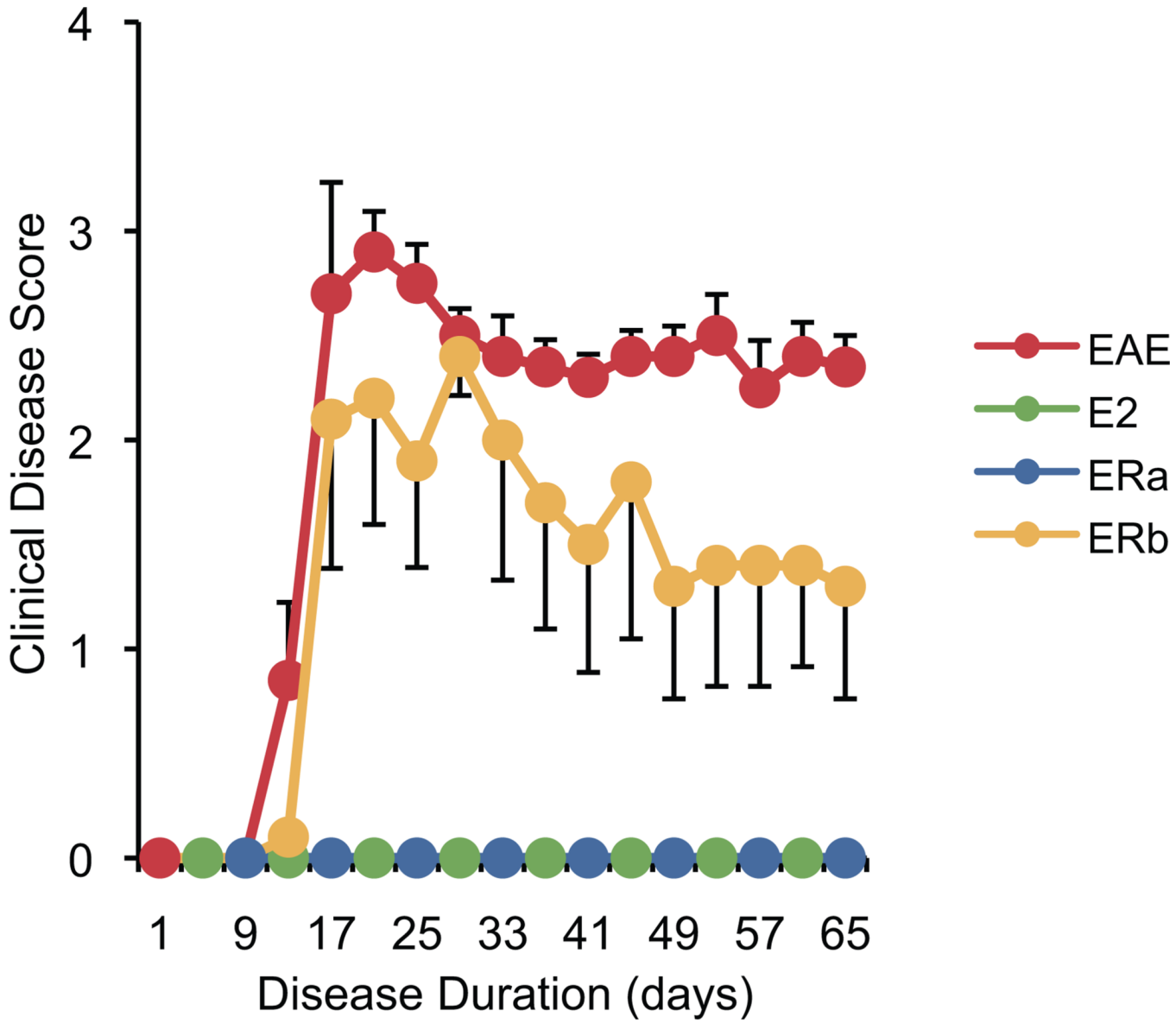

Fig. 1.

Clinical disease course. A graph of the mean clinical disease score in mice with EAE plotted against disease duration. Each color represents a treatment group (red for vehicle-treated EAE mice (EAE), green for estradiol-treated EAE mice (E2), blue for ER-alpha ligand-treated EAE mice (ERa) and yellow for ER-beta ligand-treated EAE mice (ERb); for clarity colors are alternated when lines are overlaid) and is used consistently in subsequent figures. Error bars indicate SEM.

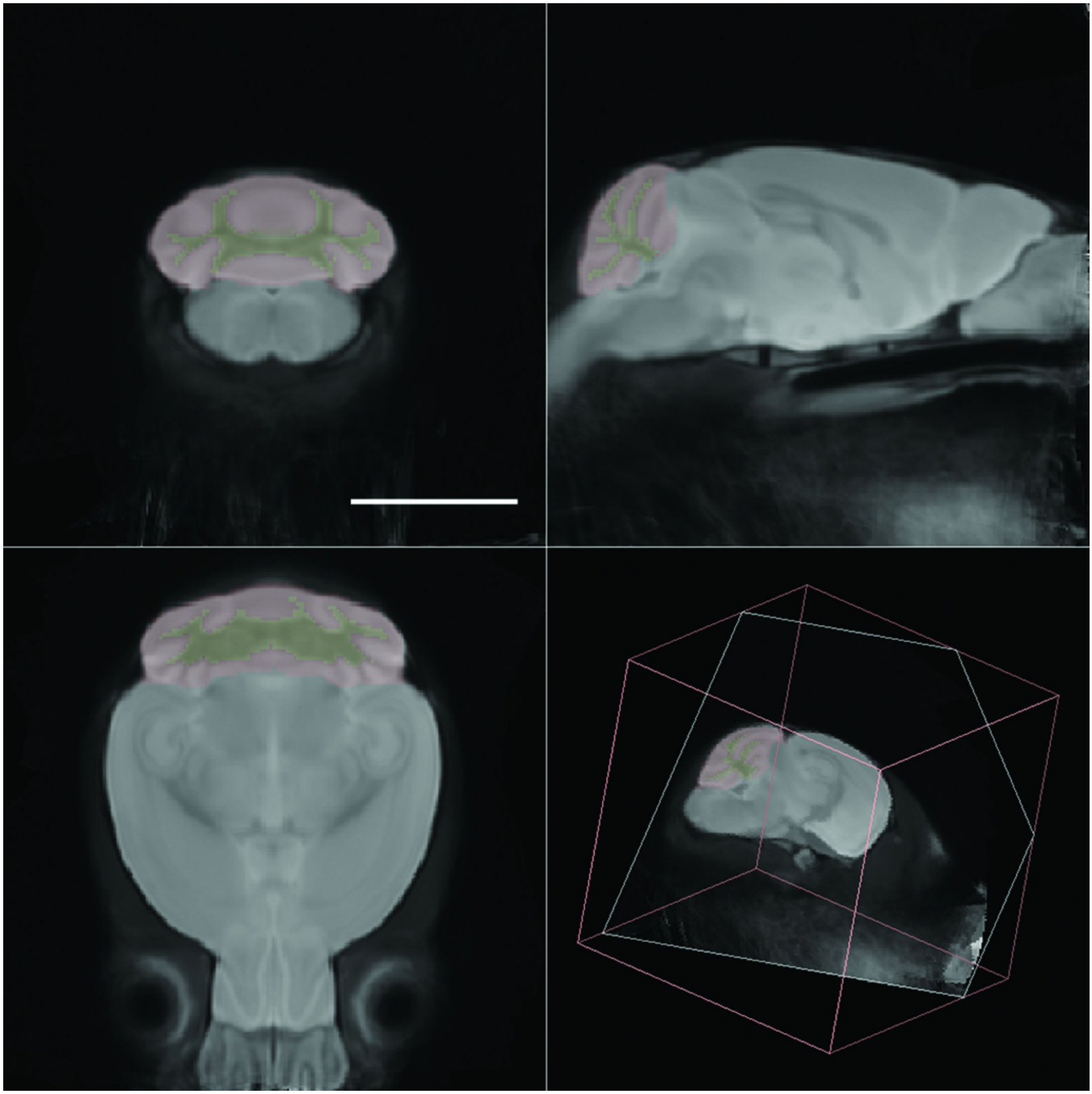

Fig. 2.
Minimum deformation atlas and delineations. A minimum deformation atlas was constructed from 30 postmortem high-resolution isotropic diffusion-weighted images of mouse brain. The anatomical delineations of the cerebellar cortex (red) and cerebellar white matter (yellow) are overlaid on the image. Scale bar = 5 mm.

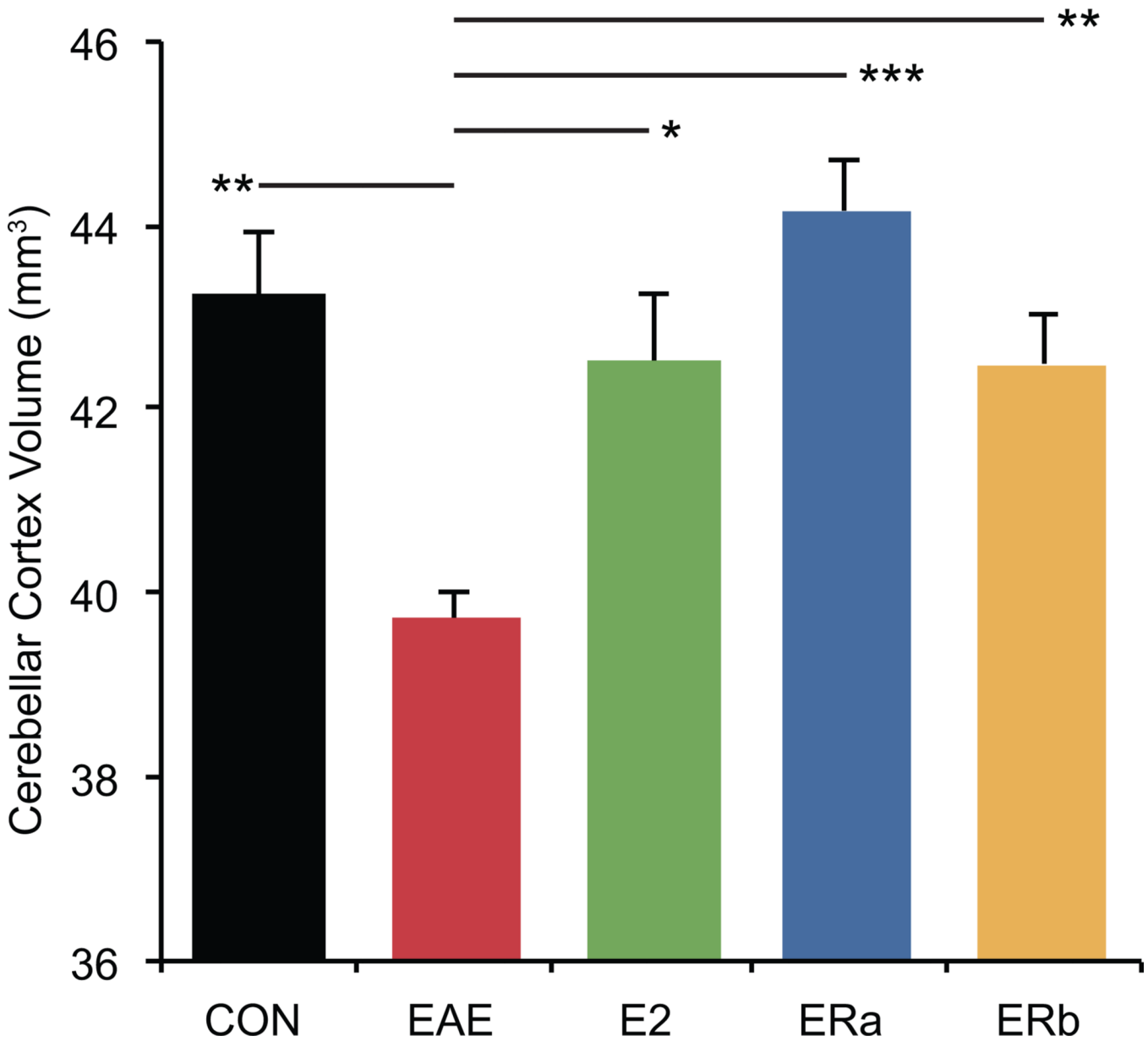

Fig. 3.

Estrogen receptor ligand treatment of mice with EAE inhibits atrophy in the cerebellar cortex. A graph of the mean cerebellar cortical volume in ovarectomized vehicle-treated healthy controls (CON), ovarectomized vehicle-treated EAE mice (EAE), ovarectomized estradiol-treated EAE mice (E2), ovarectomized ER-alpha ligand-treated EAE mice (ERa) and ovarectomized ER-beta ligand-treated EAE mice (ERb). Error bars indicate SEM. Asterisks indicate statistical significance (* $p < 0.01$, ** $p < 0.0001$). All significant differences survive the application of the Bonferroni correction for post hoc testing.

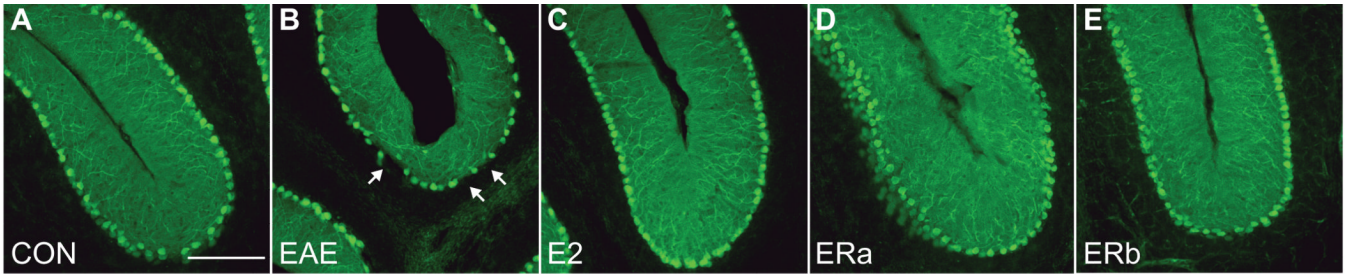

Fig. 4.

Purkinje cell staining in the cerebellum. Calbindin-28K immunostained confocal images at 10X magnification from the cerebellum of an ovarectomized vehicle-treated healthy control mouse (A), an ovarectomized vehicle-treated mouse with EAE (B), an ovarectomized E2-treated mouse with EAE (C), an ovarectomized ER-alpha ligand-treated mouse with EAE (D) and an ovarectomized ER-beta ligand-treated mouse with EAE (E). Scale bar = 80 um.

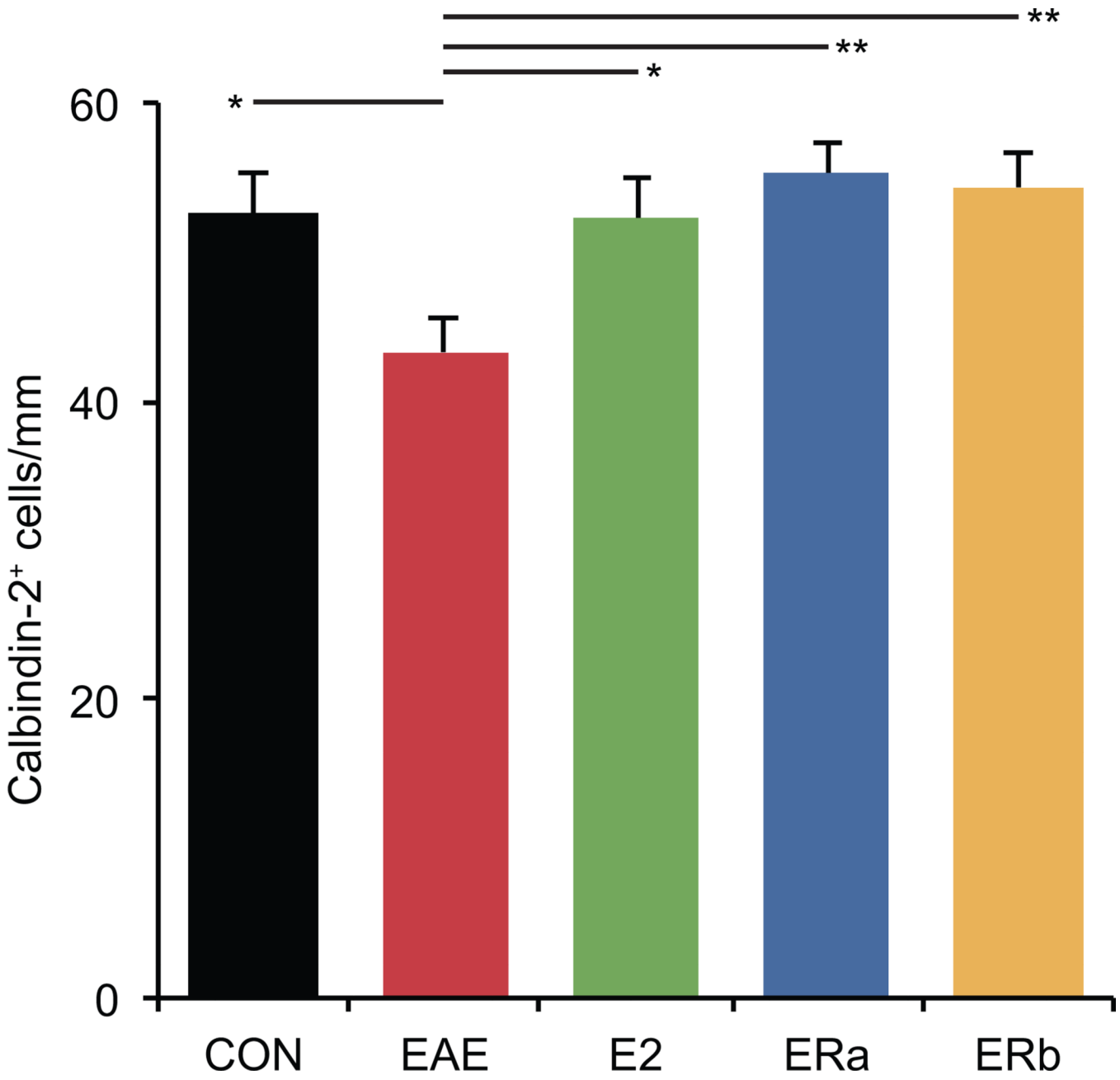

Fig. 5.

Estrogen receptor ligand treatment of mice with EAE inhibits Purkinje cell loss. A graph of the number of calbindin-2^+ cells in the cerebella of ovarectomized vehicle-treated healthy controls (CON), ovarectomized vehicle-treated EAE mice (EAE), ovarectomized E2-treated EAE mice (E2), ovarectomized ER-alpha ligand-treated EAE mice (ERa) and ovarectomized ER-beta ligand-treated EAE mice (ERb). Error bars indicate SEM. Asterisks indicate statistical significance (* $p < 0.01$, ** $p < 0.001$, *** $p < 0.0001$, **** $p > 0.00001$). All significant differences survive the application of the Bonferroni correction for post hoc testing.

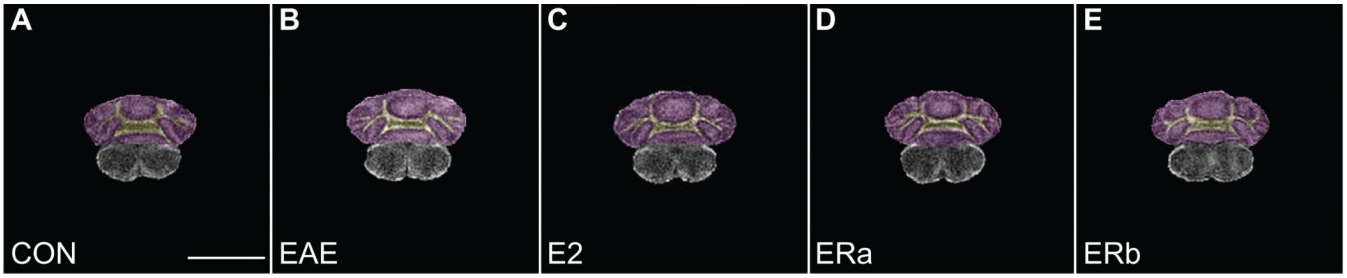

Fig. 6.

Fractional anisotropy in the cerebellum. Fractional anisotropy images derived from diffusion tensor images of the cerebellum of an ovarectomized vehicle-treated healthy control mouse (A), an ovarectomized vehicle-treated mouse with EAE (B), an ovarectomized E2-treated mouse with EAE (C), an ovarectomized ER-alpha ligand-treated mouse with EAE (D) and an ovarectomized ER-beta ligand-treated mouse with EAE (E). The anatomical delineations of the cerebellar cortex (magenta) and cerebellar white matter (yellow) are overlaid on the image. Scale bar = 5 mm.

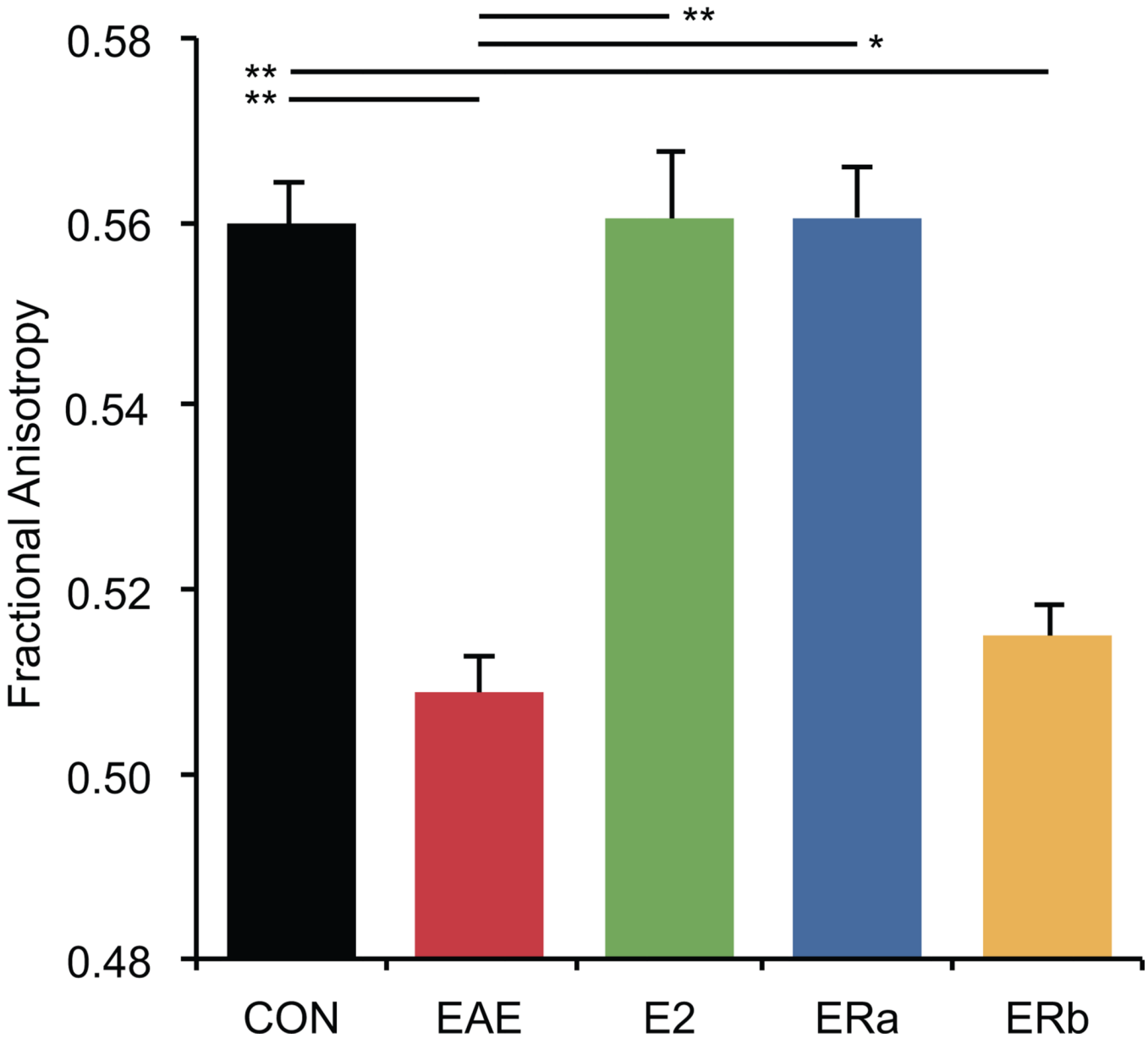

Fig. 7.

Fractional anisotropy is reduced in vehicle-treated and ER-beta ligand-treated, but not in estradiol-treated or ER-alpha ligand-treated mice with EAE. A graph of the mean fractional anisotropy in the cerebellar white matter of ovarectomized vehicle-treated healthy controls (CON), ovarectomized vehicle-treated EAE mice (EAE), ovarectomized estradiol-treated EAE mice (E2), ovarectomized ER-alpha ligand-treated EAE mice (ERa) and ovarectomized ER-beta ligand-treated EAE mice (ERb). Error bars indicate SEM. Asterisks indicate statistical significance (* $p < 0.01$, ** $p < 0.001$, *** $p < 0.0001$, **** $p > 0.00001$). All significant differences survive the application of the Bonferroni correction for post hoc testing.

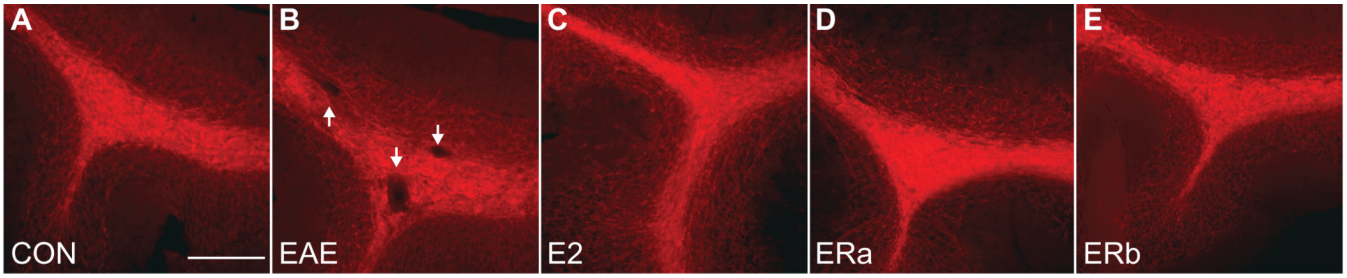

Fig. 8.

Myelin basic protein staining in the cerebellum. Myelin basic protein immunostained confocal images at 10X magnification from the cerebellum of an ovarectomized vehicle-treated healthy control mouse (A), an ovarectomized vehicle-treated EAE mouse (B), an ovarectomized E2-treated EAE mouse (C), an ovarectomized ER-alpha ligand-treated EAE mouse (D) and an ovarectomized ER-beta ligand-treated EAE mouse (E). Arrows indicate demyelinated lesions. Scale bar = 80 um.

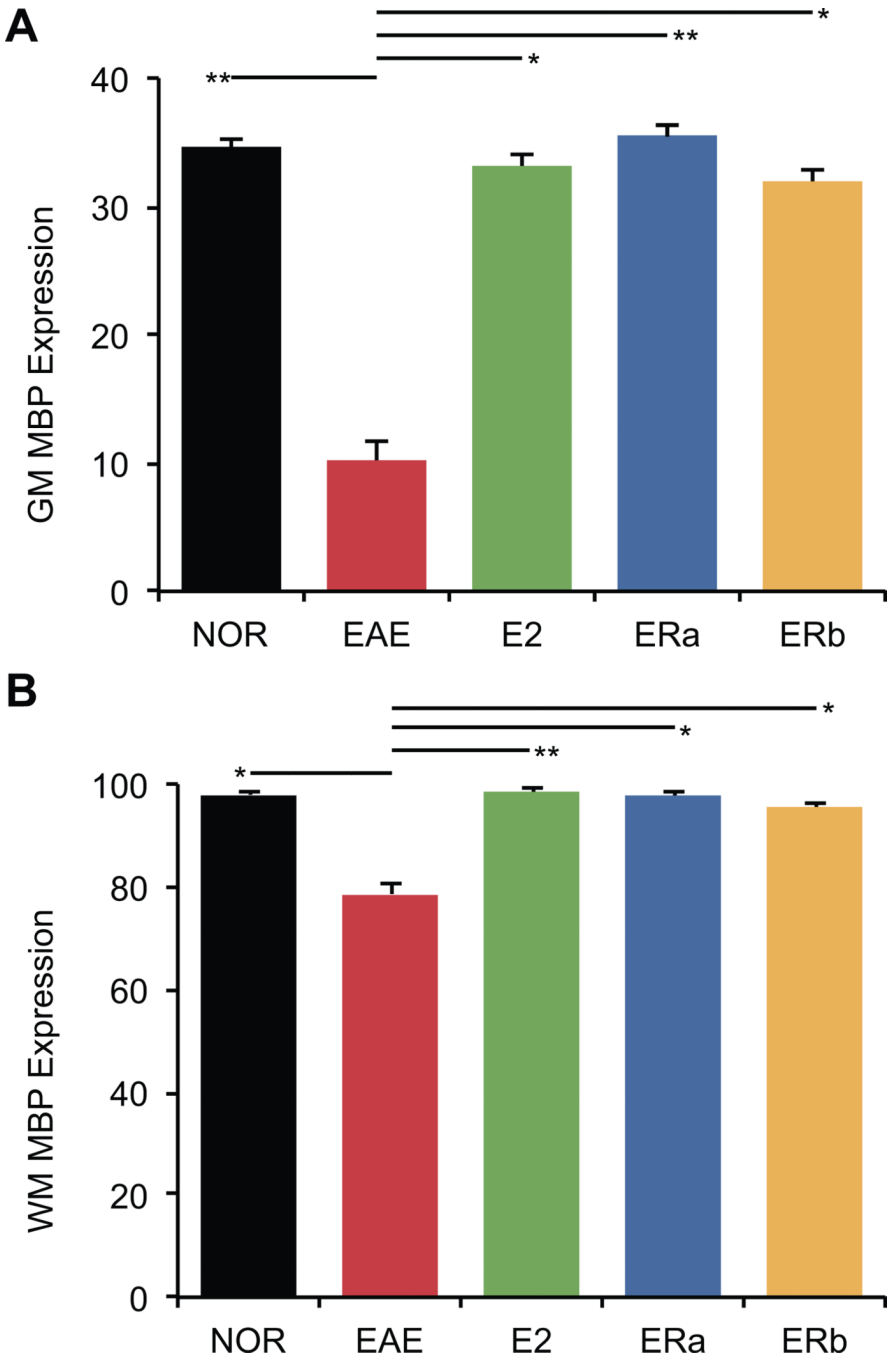

Fig. 9.

Estrogen receptor ligand treatment of mice with EAE preserves myelin staining in the cerebellum. (A) A graph of the mean myelin-staining in the cerebellar white matter of ovarectomized vehicle-treated healthy controls (CON), ovarectomized vehicle-treated EAE mice (EAE), ovarectomized E2-treated EAE mice (E2), ovarectomized ER-alpha ligand-treated EAE mice (ERa) and ovarectomized ER-beta ligand-treated EAE mice (ERb). (B) A graph of the mean myelin-staining in the cerebellar gray matter of ovarectomized vehicle-treated healthy controls (CON), ovarectomized vehicle-treated EAE mice (EAE), ovarectomized E2-treated EAE mice (E2), ovarectomized ER-alpha ligand-treated EAE mice (ERa) and ovarectomized ER-beta ligand-treated EAE mice (ERb). Error bars indicate

SEM. Asterisks indicate statistical significance (* $p < 0.01$, ** $p < 0.001$, *** $p < 0.0001$, **** $p > 0.00001$). All significant differences survive the application of the Bonferroni correction for post hoc testing.

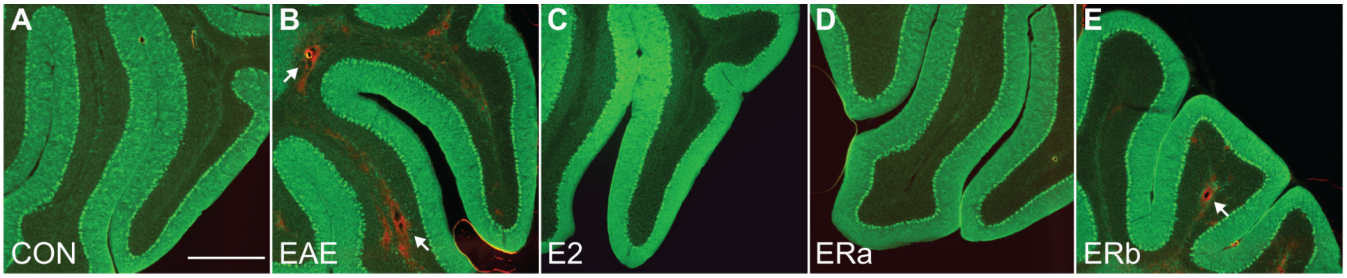

Fig. 10.

Inflammatory cell staining in the cerebellum. CD45 immunostained confocal images at 4X magnification from the cerebellum of an ovarectomized vehicle-treated healthy control mouse (A), an ovarectomized vehicle-treated EAE mouse (B), an ovarectomized E2-treated EAE mouse (C), an ovarectomized ER-alpha ligand-treated EAE mouse (D) and an ovarectomized ER-beta ligand-treated EAE mouse (E). Arrows indicate cellular infiltrate. Scale bar = 200 um.

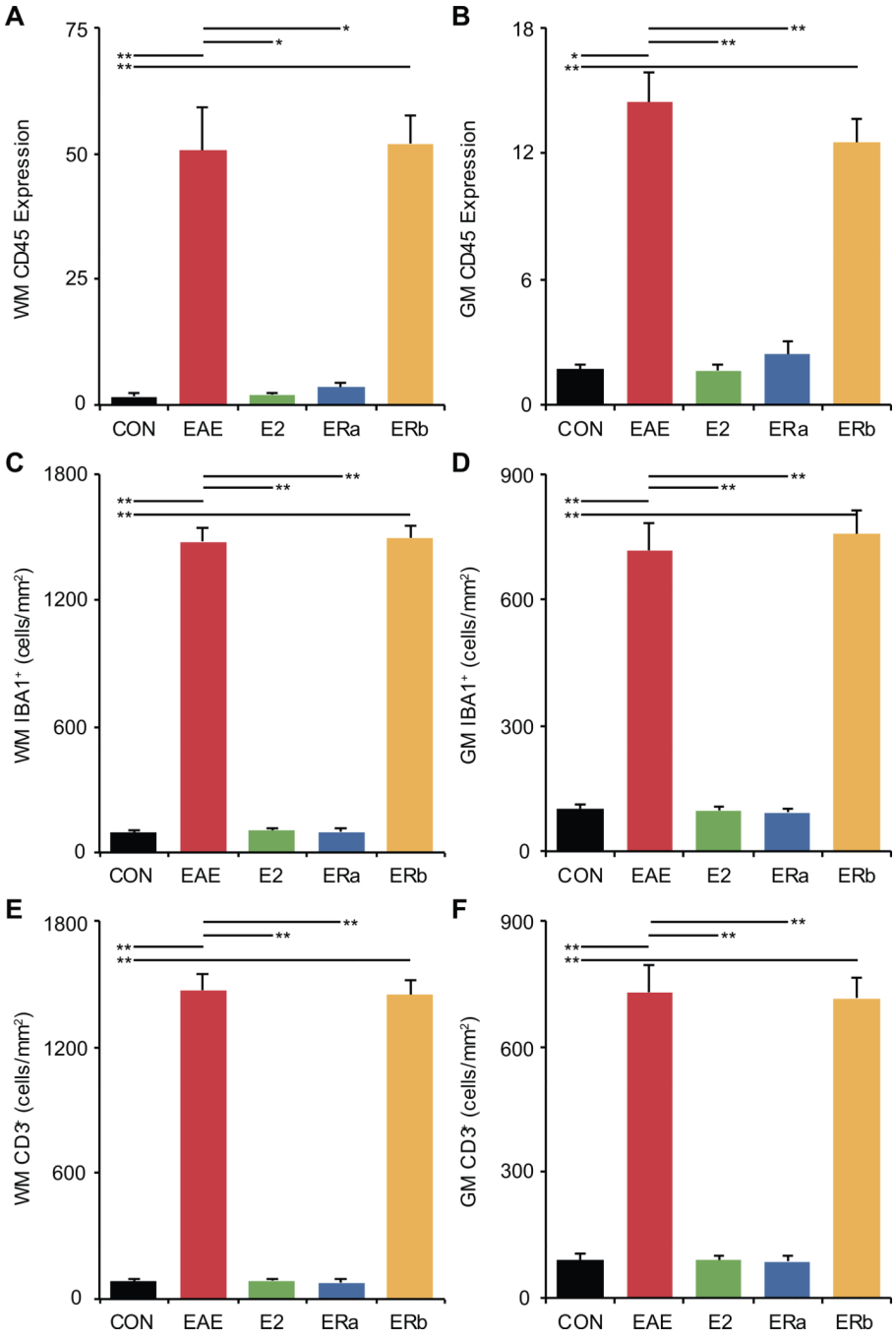

Fig. 11.

Inflammation is increased in vehicle-treated and ER-beta ligand-treated, but not in ER-alpha ligand-treated mice with EAE. (A) A graph of the mean CD45-staining in the cerebellar gray matter of ovarectomized vehicle-treated healthy controls (CON), ovarectomized vehicle-treated EAE mice (EAE), ovarectomized E2-treated EAE mice (E2), ovarectomized ER-alpha ligand-treated EAE mice (ERa) and ovarectomized ER-beta ligand-treated EAE mice (ERb). (B) A graph of the mean CD45-staining in the cerebellar white matter of ovarectomized vehicle-treated healthy controls, ovarectomized vehicle-treated EAE mice, ovarectomized E2-treated EAE mice, ovarectomized ER-alpha ligand-treated EAE mice and ovarectomized ER-beta ligand-treated EAE mice. (C) A graph of the mean number of

IBA1$^+$ cells per square mm in the cerebellar white matter of ovarectomized vehicle-treated healthy controls, ovarectomized vehicle-treated EAE mice, ovarectomized E2-treated EAE mice, ovarectomized ER-alpha ligand-treated EAE mice and ovarectomized ER-beta ligand-treated EAE mice. (D) A graph of the number of IBA1$^+$ cells per square mm in the cerebellar gray matter of ovarectomized vehicle-treated healthy controls, ovarectomized vehicle-treated EAE mice, ovarectomized E2-treated EAE mice, ovarectomized ER-alpha ligand-treated EAE mice and ovarectomized ER-beta ligand-treated EAE mice. (E) A graph of the mean number of CD3$^+$ cells per square mm in the cerebellar white matter of ovarectomized vehicle-treated healthy controls, ovarectomized vehicle-treated EAE mice, ovarectomized E2-treated EAE mice, ovarectomized ER-alpha ligand-treated EAE mice and ovarectomized ER-beta ligand-treated EAE mice. (F) A graph of the number of CD3$^+$ cells per square mm in the cerebellar gray matter of ovarectomized vehicle-treated healthy controls, ovarectomized vehicle-treated EAE mice, ovarectomized E2-treated EAE mice, ovarectomized ER-alpha ligand-treated EAE mice and ovarectomized ER-beta ligand-treated EAE mice. Error bars indicate SEM. Asterisks indicate statistical significance (* $p < 0.01$, ** $p < 0.001$, *** $p < 0.0001$, **** $p > 0.00001$). All significant differences survive the application of the Bonferroni correction for post hoc testing.

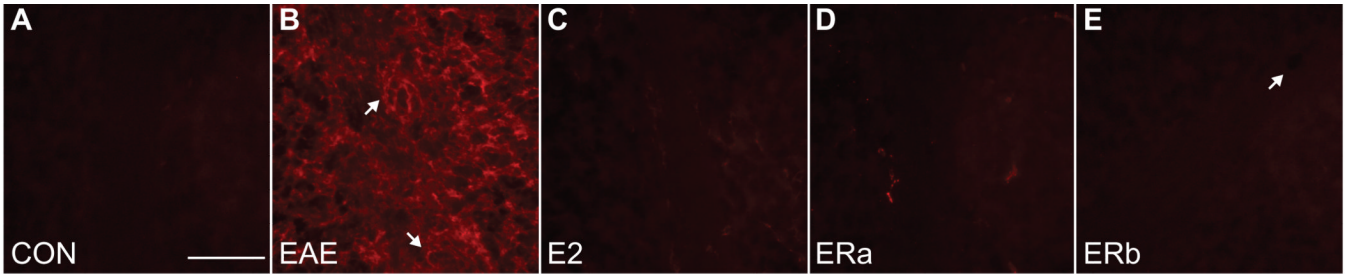

Fig. 12.

Beta-amyloid precursor protein staining in the cerebellum. Beta-APP (red) immunostained confocal images at 40X magnification from the cerebellum of an ovarectomized vehicle-treated healthy control mouse (A), an ovarectomized vehicle-treated EAE mouse (B), an ovarectomized E2-treated EAE mouse (C), an ovarectomized ER-alpha ligand-treated EAE mouse (D) and an ovarectomized ER-beta ligand-treated EAE mouse (E). Arrows in (B) indicate lesions centered on blood vessels, whereas the arrow in (E) indicates a blood vessel without a surrounding lesion. Scale bar = 20 um.

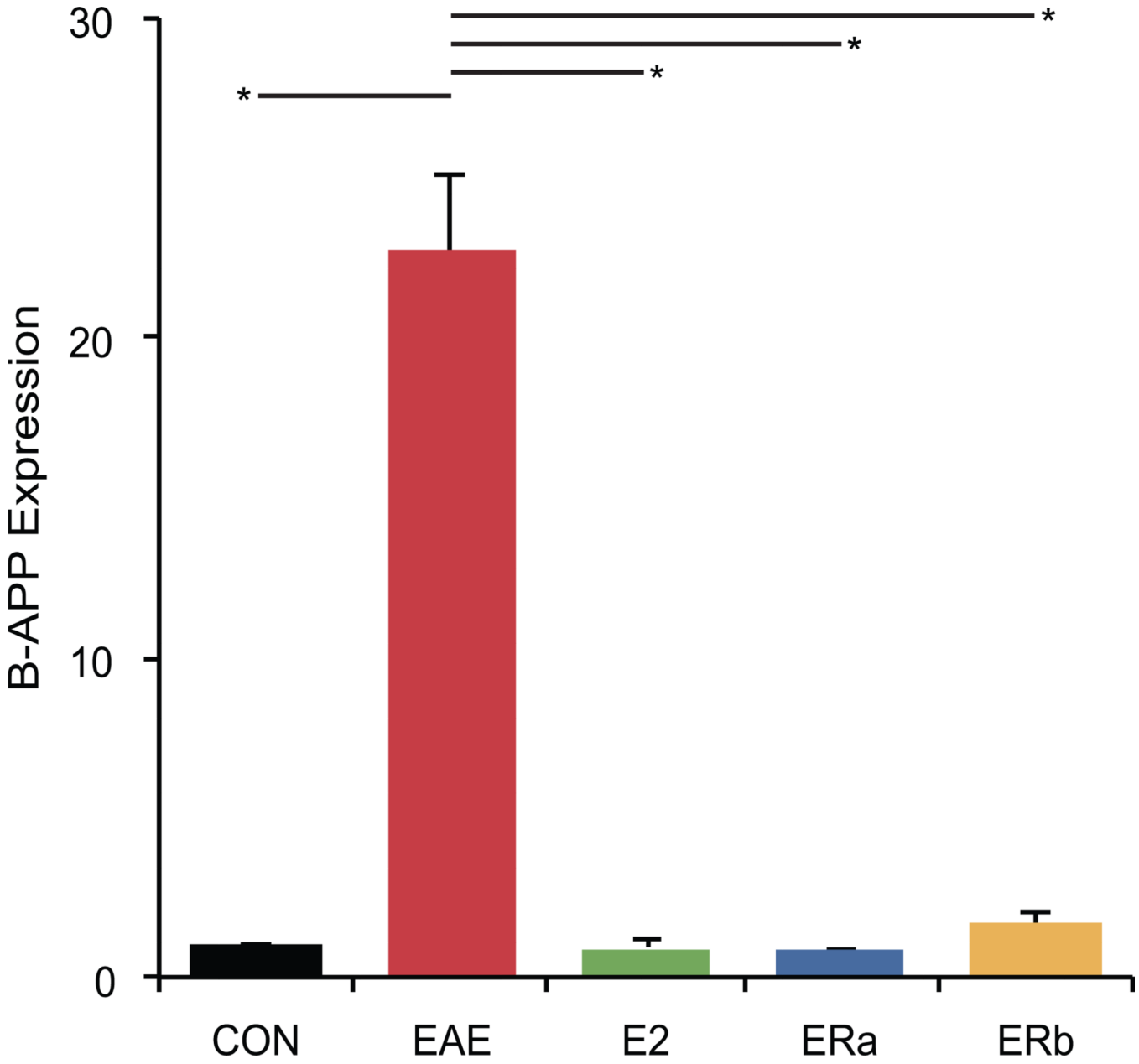

Fig. 13.

Estrogen receptor ligand treatment of mice with EAE abrogates beta-amyloid precursor protein staining in the cerebellum. A graph of the mean beta-APP-staining in the cerebellar white matter of ovarectomized vehicle-treated healthy controls (CON), ovarectomized vehicle-treated EAE mice (EAE), ovarectomized E2-treated EAE mice (E2), ovarectomized ER-alpha ligand-treated EAE mice (ERa) and ovarectomized ER-beta ligand-treated EAE mice (ERb). Error bars indicate SEM. Asterisks indicate statistical significance (* $p < 0.0005$). All significant differences survive the application of the Bonferroni correction for post hoc testing.

Table 1

Summary of imaging and histology results.

	CON	EAE	E2	ERa	ERb
Volumetry	43.2 (0.7)	39.7 (0.3)	42.5 (0.5)	44.2 (0.6)	42.5 (0.7)
Fractional Anisotropy	0.560 (0.005)	0.509 (0.004)	0.560 (0.007)	0.561 (0.006)	0.515 (0.003)
Purkinje Cell Number	52.6 (2.8)	43.3 (2.4)	52.2 (2.8)	55.2 (2.2)	54.3 (2.3)
MBP GM	34.53 (0.68)	10.19 (1.44)	33.12 (1.01)	35.68 (0.90)	31.95 (0.78)
MBP WM	97.95 (0.37)	78.61 (2.06)	98.35 (0.76)	97.52 (1.12)	95.2 (1.04)
CD45 GM	1.7 (0.3)	14.4 (1.4)	1.6 (0.3)	2.4 (0.6)	12.5 (1.2)
CD45 WM	1.7 (0.5)	50.7 (8.4)	2.0 (0.2)	3.5 (1.0)	52.0 (5.6)
IBA1 GM	102.0 (8.9)	718.6 (63.8)	97.6 (9.5)	93.6 (8.9)	757.2 (56.1)
IBA1 WM	94.0 (12.8)	1481.2 (67.8)	102.4 (12.2)	98.8 (11.8)	1497.8 (61.8)
CD3 GM	89.6 (13.8)	729.6 (63.8)	89.8 (9.2)	87.6 (11.4)	716.2 (48.6)
CD3 WM	82.4 (12.4)	1470.0 (76.5)	87.6 (9.5)	78.0 (12.8)	1449.0 (65.7)
Beta-APP	1.0 (0.1)	22.7 (2.4)	0.9 (0.2)	0.8 (0.1)	1.6 (0.5)

Values are expressed as mean (SEM).